

## Chapter 6

# Toward Numerical Simulation

This chapter aims at reviewing the fundamentals of numerical simulation for the physical processes described in the previous chapters.

The hypothesis of dilution states that the time evolution of concentrations can be split from the time evolution of the meteorological fields (wind velocity, air density, temperature, humidity). The time evolution of concentrations is then given by an advection-diffusion-reaction partial differential equation, the so-called equation of *reactive dispersion*. Advection corresponds to wind transport, diffusion to turbulent mixing, and reactions to physical and chemical processes. The three-dimensional numerical models that solve these equations are the so-called *chemistry-transport models* (CTM). Such models are the basis of any state-of-the-science modeling systems for air quality.

Numerical simulation of the dispersion equation is a challenging issue. For example, the dimension of the partial differential equations can be up to tens of chemical species (Table 6.1). The characteristic timescales also reveal a wide range: from fractions of seconds for the fastest chemical reactions or condensation onto the finest aerosols, to hours, days or years for the most stable species. This induces the so-called numerical *stiffness*, one of the most difficult issues for numerical simulation, with several consequences: computational burden, use of tailored numerical solvers for the time integration, and so on.

This chapter is organized as follows. The reactive dispersion equation is formulated for averaged variables in Sect. 6.1. The underlying model hierarchy (from Gaussian models to three-dimensional Eulerian chemistry-transport models) is then presented. Section 6.2 is devoted to the fundamentals of numerical analysis required for the chemistry-transport models. Attention is paid to *operator splitting* in Sect. 6.2.1, time integration of chemical kinetics in Sect. 6.2.2, and advection in Sect. 6.2.3. The numerical simulation of aerosol dynamics is investigated in Sect. 6.3. To conclude, high-level methods, such as the propagation of uncertainties or data assimilation (coupling between the model outputs and the measured data in order to constrain the simulation), are briefly introduced in Sect. 6.4.

**Table 6.1** Number of chemical variables per grid cell in a CTM for different applications (accidental release, photochemistry, multiphase chemistry). Note that photochemistry, cloud chemistry and aerosols have to be taken into account for a multiphase model

Application	Number of species
Passive tracer	1
Photochemistry	50–100
Cloud chemistry	10–50
Aerosols	$\geq 100$ (20 times, <i>a minima</i> , 5 size sections)

## 6.1 Reactive Dispersion Equation

### 6.1.1 Dilution and Off-Line Coupling

It is desired to describe the evolution of trace species concentrations in the atmosphere: the trace species can be chemical species, biological compounds or radionuclides in the gas and particulate phase.

The evolution of the reactive fluid is given by the reactive Navier-Stokes equations, defined by adding species continuity equations to the Navier-Stokes equations (Sect. 3.5). When solved, this coupled model is usually referred to as an *on-line* model.

Evolution of meteorological fields and evolution of species concentrations are usually decoupled: this is the so-called *dilution* hypothesis. This can be motivated when the contributions of trace species to the evolution of temperature (or of internal energy) can be approximated by a constant value. A first (direct) contribution is related to the heat fluxes generated by chemical reactions. A second (indirect) contribution is related to interactions between atmospheric matter and solar and terrestrial radiations (Chap. 2).

In a first approximation, the first contribution can be neglected in the troposphere. The second contribution plays a leading role in atmospheric dynamics: it can be neglected for air quality studies at regional scales but not at a global scale for long-term climate studies.

In the sequel, we assume that the dilution hypothesis is satisfied. The meteorological fields (wind velocity, temperature, density, relative humidity, etc.) are supposed to be computed by a meteorological model in a preprocessing step. They are then given as input data for the dispersion equations of the trace species. This approach is usually referred to as *off-line coupling*.

### 6.1.2 Advection-Diffusion-Reaction Equations

**Concentrations** The processes that govern evolution of the atmospheric trace species are shown in Fig. 6.1. The species  $X_i$  is represented by a concentration,

$c_i$ , expressed in a number of moles (or of molecules) per air volume, or by a mass concentration expressed in units of mass per air volume.

Let us consider a gas-phase species. The evolution of  $c_i$  is then given by a system of partial differential equations (PDE),

$$\frac{\partial c_i}{\partial t} + \text{div}[V(x, t)c_i] = \text{div}(K_{molec} \nabla c_i) + \chi_i[c, T(x, t), t] + S_i(x, t) - \Lambda_i c_i, \quad (6.1)$$

where  $x$  and  $t$  stand for the spatial and time coordinates, respectively, and  $c$  is the vector of concentrations.

Different data sets are required:

- *Meteorological fields.*

$V(x, t)$  is the wind velocity,  $K_{molec}$  is the molecular-diffusion matrix (we take into account, *a priori*, intermolecular diffusion),  $T(x, t)$  is the temperature.

- *Emission data.*

$S_i(x, t)$  is the source term for species  $X_i$ : it describes the point emissions (typically a chimney).

- *Physical and chemical parameterizations.*

$\chi_i$  stands for the chemical source term of  $X_i$  in the gaseous phase (Chap. 4). It depends on concentrations, temperature, radiative actinic flux and relative humidity (the last two variables are omitted for the sake of clarity).

Scavenging terms (for wet removal by precipitations and clouds) are usually parameterized by the term  $-\Lambda_i c_i$ . The scavenging coefficient,  $\Lambda_i$ , is a function of the meteorological fields (liquid water content or rain intensity) and of several microphysical variables (Sect. 5.3.2).

**Mixing Ratio** Another description is based on the mixing ratio, written as  $C_i = c_i/\rho$  (expressed in  $\text{mol mol}^{-1}$ ). The air density satisfies the continuity equation (Chap. 3)

$$\frac{\partial \rho}{\partial t} + \text{div}(\rho V) = 0. \quad (6.2)$$

It is then easy to prove (Exercise 6.1) that the evolution of  $C_i$  is given by

$$\frac{\partial C_i}{\partial t} + V \cdot \nabla C_i = \frac{1}{\rho} \text{div}(K_{molec} \nabla(\rho C_i)) + \frac{\chi_i(\rho C, T(x, t), t) + S_i(x, t)}{\rho} - \Lambda_i C_i. \quad (6.3)$$

**Exercise 6.1** (Mixing Ratio and Mass Consistency) We consider the case of pure advection by the wind. Formulate the evolution equation of the mixing ratio. Prove the *mass consistency* property: a passive tracer that is initially well mixed (namely with a homogeneous mixing ratio) remains well mixed.

**Solution:**

It is straightforward to obtain:

$$\frac{\partial C_i}{\partial t} = \frac{1}{\rho} \frac{\partial c_i}{\partial t} - \frac{c_i}{\rho^2} \frac{\partial \rho}{\partial t} = \frac{-\text{div}(V c_i)}{\rho} + \frac{c_i}{\rho^2} \text{div}(\rho V) = \frac{-\text{div}(\rho V C_i) + C_i \text{div}(\rho V)}{\rho}$$

$$= -\left(V \cdot \nabla C_i + \frac{C_i}{\rho} \operatorname{div}(\rho V)\right) + \frac{C_i}{\rho} \operatorname{div}(\rho V) = -V \cdot \nabla C_i.$$

It is then easy to check the mass consistency property: if  $C_i(t=0) = k$ , with  $k$  a constant,  $C_i(t) = k$  is the unique solution for the advection equation.

To know more ([138]):

B. SPORTISSE, D. QUÉLO, AND V. MALLET, *Impact of mass consistency errors for atmospheric dispersion*, Atmos. Env., **41** (2007), pp. 6132–6142

### 6.1.3 Averaged Models and Closure Schemes

Equation (6.1) is only valid at the “microscopic” scale (at least in a continuum description) but cannot be used, as such, for turbulent flows. As it is illustrated in Chap. 3, it is not possible to simulate all scales in a three-dimensional case and averaging approaches are necessary.

We assume that the fields (meteorological fields, trace species concentrations) can be decomposed as  $\Psi = \langle \Psi \rangle + \Psi'$  with  $\langle \Psi \rangle$  an averaged value and  $\Psi'$  a fluctuation. We do not detail the averaging operator: note that it is supposed to satisfy commutation of derivation (with respect to time and space) and  $\langle \Psi' \rangle = 0$ .

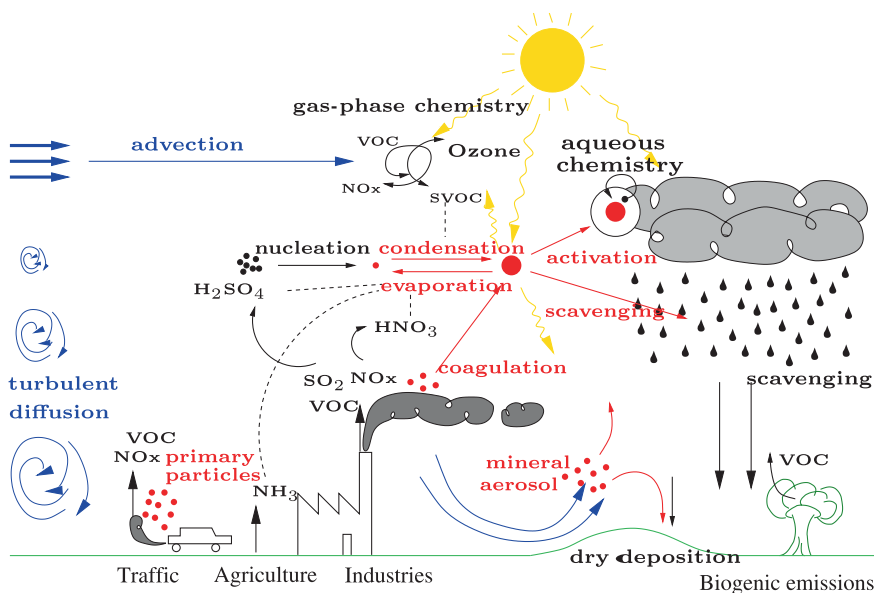


Fig. 6.1 Sketch of the processes described in a tropospheric chemistry-transport model

When applied to (6.1), this decomposition leads, after having averaged the resulting equation, to

$$\begin{aligned} \frac{\partial \langle c_i \rangle}{\partial t} + \text{div}(\langle V(x, t) \rangle \langle c_i \rangle) \\ = \text{div}(K_{molec} \nabla \langle c_i \rangle) + \langle \chi_i(c, T(x, t), t) \rangle \\ + \langle S_i(x, t) \rangle - \langle \Lambda_i c_i \rangle - \text{div}(\langle c'_i V' \rangle). \end{aligned} \quad (6.4)$$

The key intermediate step is  $\langle c_i + c'_i \rangle \langle V + V' \rangle = \langle V \rangle \langle c_i \rangle + \langle c'_i V' \rangle$ .

Note that the *linear* terms are not modified in the averaged equation. The *non-linear* terms (here in a quadratic form) generate *correlations* (averaged products of fluctuations). A *closure scheme* for the averaged equations consists in expressing these correlations as a function of the *resolved* variables (the averaged fields).

The two main processes requiring a closure scheme are wind advection (vertical turbulent flux) and chemical production (segregation effect).

### 6.1.3.1 Turbulent Flux

The averaging of the continuity equation for species  $X_i$  introduces a new term associated to wind advection,  $\text{div}\langle c'_i V' \rangle$ . This term can be viewed as a turbulent flux.

The closure scheme is usually based on the so-called *K-theory*, by analogy with molecular diffusion (Chap. 3). The parameterization is then given for a field  $\Psi$  by

$$\langle \Psi' V' \rangle = -K_{turb}^{\Psi}(x, t) \nabla \langle \Psi \rangle, \quad (6.5)$$

with  $K_{turb}^{\Psi}$  the eddy diffusion matrix. In practice  $K_{turb}^{\Psi}$  is a function of the meteorological fields and their gradients, and it depends on space and time.

The application of this parameterization to the concentration  $c_i$  or to the mixing ratio  $C_i$  does not lead to the same result. Actually, it is more relevant to apply the parameterization to the mixing ratio,

$$\langle C'_i V' \rangle = -K_{turb} \nabla \langle C_i \rangle. \quad (6.6)$$

The fluctuation of density is usually neglected ( $\rho' = 0$ ). As  $c_i = \rho C_i$ , one gets  $c'_i V' \simeq \langle \rho \rangle C'_i V'$  and  $\langle c_i \rangle \simeq \langle \rho \rangle \langle C_i \rangle$ . The resulting parameterization for the concentration is then

$$\langle c'_i V' \rangle = -\langle \rho \rangle K_{turb} \nabla \left( \frac{\langle c_i \rangle}{\langle \rho \rangle} \right). \quad (6.7)$$

The advantage of this parameterization is that the mass consistency property is still satisfied (Exercise 6.1). If  $\langle c_i \rangle / \langle \rho \rangle$  is initially homogeneous, the homogeneity is conserved for the averaged equation. This is easy to prove since the averaged equation is exactly the initial equation, as the turbulent flux is equal to zero. Such a result would not have been obtained by applying the *K-theory* to the concentration.

The turbulent diffusion matrix is supposed to be the same one for all species, and inter-molecular turbulent diffusion is neglected. The matrix  $K_{turb}$  is usually a

*diagonal* matrix: we write  $K_x$ ,  $K_y$  and  $K_z$  the eddy diffusion coefficients for the directions  $x$ ,  $y$  and  $z$ , respectively.

In practice,  $K_{turb}$  is much higher than  $K_{molec}$  (about  $10^{-5} \text{ m}^2 \text{ s}^{-1}$ ): the diffusion flux is chiefly the turbulent diffusion flux except in a thin laminar layer just above the ground.

Moreover, the horizontal diffusion terms can be usually neglected since it dominates the horizontal advection transport. They are somehow not well parameterized and are exceeded by the *numerical diffusion* of advection schemes (Sect. 6.2.3 and Exercise 6.6). To conclude, only the eddy vertical diffusion is usually taken into account. It is described by  $K_z$  (typically about  $10 \text{ m}^2 \text{ s}^{-1}$ ).

### 6.1.3.2 Segregation Effect

The averaging procedure leads to a closure problem for nonlinear chemical kinetics. The rate of a bimolecular chemical reaction with reactants  $X_i$  and  $X_j$  (Chap. 4) is

$$\langle c_i c_j \rangle = \langle c_i \rangle \langle c_j \rangle + \langle c'_i c'_j \rangle, \quad (6.8)$$

where the correlation term  $\langle c'_i c'_j \rangle$  is not resolved. This term is usually neglected. This assumption is sometimes referred to as the *well-stirred tank reactor* hypothesis. In this case we obtain

$$\langle \chi(c) \rangle \simeq \chi(\langle c \rangle). \quad (6.9)$$

This assumption is valid only if the characteristic timescales of chemical kinetics are much higher than the timescales of turbulent mixing (Exercise 6.2).

Note that the correlation term is sometimes called a *segregation* term. From this viewpoint, we can also write

$$\langle c_i c_j \rangle = \langle c_i \rangle \langle c_j \rangle (1 + I_s), \quad I_s = \frac{\langle c'_i c'_j \rangle}{\langle c_i \rangle \langle c_j \rangle}, \quad (6.10)$$

with  $I_s$  the *segregation intensity*. It is easy to check that  $I_s \geq -1$  due to the positivity of concentrations.

**Exercise 6.2 (Damköhler Number)** We define a Damköhler number,  $Da$ , as the ratio of a characteristic timescale of chemical kinetics to a characteristic timescale of turbulent mixing. Comment the different regimes defined by the magnitude of  $Da$ . Classify a few chemical species.

**Solution:**

When  $Da \ll 1$  (typically for long-lived VOCs, PAN, etc.), we can consider that the environment is well mixed: there is no segregation. When  $Da \gg 1$ , chemical kinetics is at equilibrium before turbulence mixing of pollutants: chemical kinetics first governs the evolution of species (for short-lived species, such as radicals, Exercise 6.5: typically OH and HO<sub>2</sub>). When  $Da \sim 1$ , the characteristic timescales of chemical kinetics and of turbulent mixing have similar values and the processes are strongly coupled: the laminar assumption is no longer valid

and the segregation effect has to be taken into account (typically for  $O_3$  and  $NO_2$ ).

*To know more* ([147]):

J. VILA-GUERAU DE ARELLANO, A. DOSIO, J. VINUESA, A. HOLTSAG, AND S. GALMARINI, *The dispersion of chemically reactive species in the atmospheric boundary layer*, Meteor. Atmos. Phys., **87** (2004)

If two species are not correlated,  $I_s = 0$ . Otherwise, the well-stirred tank reactor hypothesis can lead to a deviation to the effective chemical source term, defined at the *model resolution*. The classical illustration is the titration reaction for ozone and nitrogen monoxide, a decisive reaction for photochemistry (Chap. 4),



Nitrogen monoxide (NO) is emitted at ground (about 90% of  $NO_x$  emissions are in this form), while ozone ( $O_3$ ), that is transported and formed at regional scales, is dominant above the boundary layer. Henceforth NO and  $O_3$  are not well mixed: NO is rather located in *updrafts* while  $O_3$  is rather located in *downdrafts*. The segregation intensity is then negative ( $I_s < 0$ ) and the homogeneity hypothesis leads to an overestimation of the reaction rate for the titration reaction.

Figure 6.2 illustrates the heterogeneity of the reaction rate in the atmospheric boundary layer. The computation is carried out with a DNS model (*Direct Navier Stokes*), to be viewed as an “exact” computation. The zones with high values of the reaction rate (just above the ground) correspond to the zones in which the reactants are in contact (and the reaction can take place).

Similarly, measurements of the segregation intensity are shown in Fig. 6.3. The time evolution reveals peaks (in absolute value) corresponding to emissions peaks of  $NO_x$  (in the early morning and in the afternoon). The values range from 0 to  $-0.65$  and are very weak at night.

More generally, the homogeneity hypothesis is not satisfied for the fastest reactions in the vicinity of emissions. However, the parameterization of  $I_s$  is still an open question for current state-of-the-science models (in 2008).

### 6.1.3.3 Averaged Dispersion Equation

Let us assume that the segregation intensity is zero. If we neglect the correlations for the scavenging term, the averaged dispersion equation is then

$$\begin{aligned} \frac{\partial \langle c_i \rangle}{\partial t} + \text{div}(\langle V(x, t) \rangle \langle c_i \rangle) \\ = \text{div} \left[ \langle \rho \rangle K_{turb} \nabla \left( \frac{\langle c_i \rangle}{\langle \rho \rangle} \right) \right] + \chi_i(\langle c \rangle, \langle T(x, t) \rangle, t) \\ + \langle S_i(x, t) \rangle - \langle \Lambda_i \rangle \langle c_i \rangle. \end{aligned} \quad (6.11)$$

In the sequel, for the sake of clarity, the notation  $\Psi$  will stand for the averaged field.

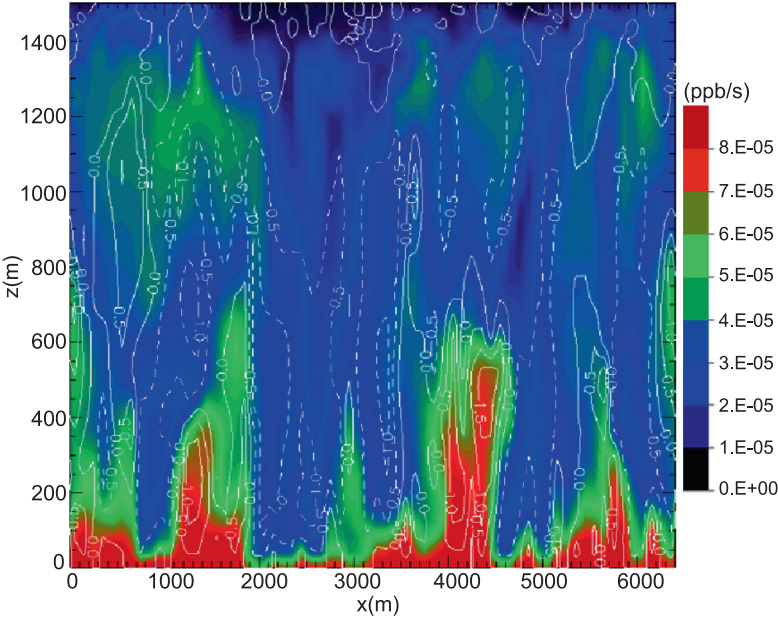
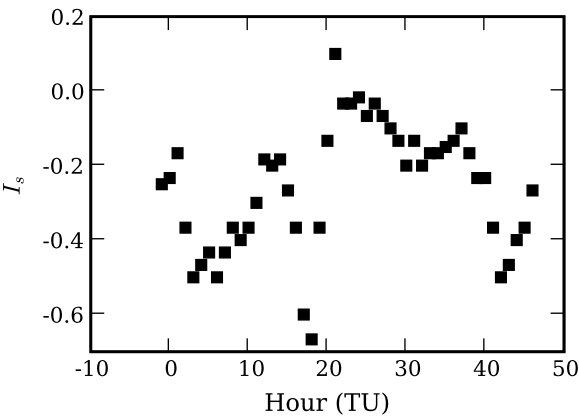


**Fig. 6.2** Reaction rate of the titration reaction  $\text{NO} + \text{O}_3$  in the atmospheric boundary layer. Computed with a DNS approach (*Direct Navier Stokes*). Credit: Jordi Vila-Guerau de Arellano ([97])

**Fig. 6.3** Time evolution of the segregation intensity for the titration reaction, at ground. The segregation intensity is estimated with a weighting approach applied to measurement stations in the Netherlands (15–16 September 1989). Source: [148]



**6.1.4 Boundary Conditions**

Initial conditions and boundary conditions have to be specified for these advection-diffusion-reaction equations.

The horizontal transport is dominated by wind advection while the vertical transport is dominated by eddy diffusion (Chap. 3). The horizontal boundary conditions



are then associated to inward-pointed wind velocities while the vertical boundary conditions are defined by diffusion fluxes.

For example, the emissions and the dry deposition define the ground boundary conditions. If  $z$  stands for the vertical coordinates, the boundary condition at  $z = 0$  reads

$$-K_z \frac{\partial c_i}{\partial z} = E_i(x, t) - v_{dep}^i(x, t)c_i. \quad (6.12)$$

The surface emission of species  $X_i$ ,  $E_i$ , depends on emission conditions (rural, urban, regional) and can be split into an anthropogenic part (e.g. related to traffic-induced emissions) and a biogenic part. The dry deposition velocity  $v_{dep}^i$  is parameterized for each chemical species according to the meteorological conditions in the surface boundary layer (Chap. 3) and to the ground type. The ground type is usually characterized by its *land use cover* (LUC) and by a specific roughness parameter (Table 3.5).

At the top of the domain ( $z = z_H$ ), namely at the interface with the so-called *free atmosphere*, the boundary condition is a null diffusion flux,

$$-K_z(x, t) \frac{\partial c_i}{\partial z} = 0. \quad (6.13)$$

### 6.1.5 Model Hierarchy

Several approaches can be used to solve (6.11). A selection of available model types is summarized in Table 6.2.

#### 6.1.5.1 Gaussian Models

**Academic Case** The most simple models are the Gaussian models ([10] for a deeper understanding). They can be introduced by an academic case. We consider a passive tracer that is emitted by a point source. The environment is supposed to have

**Table 6.2** A selection of models. A few *on-line* coupled models are used for research applications

Model type	applications
Gaussian and plume	accidental release
Particle Lagrangian	accidental release
Eulerian box	forecast (1980–2000)
Lagrangian box	impact study (1980–2000)
3D-Eulerian gas-phase CTM	forecast and impact study (1990–.)
3D-Eulerian multiphase CTM	forecast and impact study (2000–.)
<i>On-line</i> coupled model	research (2000/2005–)

a constant wind velocity ( $u$ ), aligned along the  $x$ -axis, and a constant air density. The dispersion equation for the mixing ratio is therefore

$$\frac{\partial C}{\partial t} + u \frac{\partial C}{\partial x} = K_x \frac{\partial^2 C}{\partial x^2} + K_y \frac{\partial^2 C}{\partial y^2} + K_z \frac{\partial^2 C}{\partial z^2}. \quad (6.14)$$

We investigate a point emission, emitted at  $(x, y, z) = (0, 0, 0)$  and at time  $t = 0$ . The initial condition is supposed to be  $C(x, y, z, 0) = S\delta(x)\delta(y)\delta(z)$ , with  $\delta(\cdot)$  the Dirac function at 0. In the academic case of *infinite* dimension (no boundary conditions), the exact solution is given by the Gaussian function,

$$C(x, y, z, t) = \frac{S}{(2\pi t)^{3/2} \sqrt{K_x K_y K_z}} \exp \left[ -\frac{(x - ut)^2}{4K_x t} - \frac{y^2}{4K_y t} - \frac{z^2}{4K_z t} \right]. \quad (6.15)$$

The plume extension, for instance in the  $x$  direction, is then determined by the variance  $2K_x t$  (often written as  $\sigma_x^2$ ).

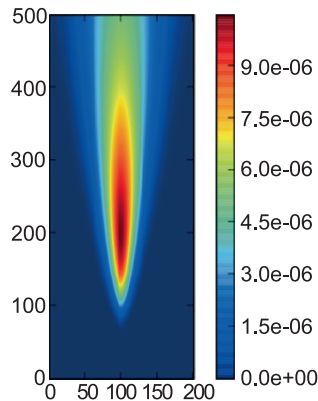
This example provides the basis for Gaussian models. In practice, there exist many situations, defined by the characteristics of sources and by ground boundary conditions. For each case, a specific analytical formula can be derived. The domain of validity is the vicinity of the sources (a few kilometers).

**Gaussian Plume Model** A *Gaussian plume model* (Fig. 6.4) is a stationary model that can be used in the case of a continuous source (continuous with respect to time), emitted at  $x = y = 0$  and at the height  $h$ , with a ground boundary condition of total reflection. The formula is

$$C(x, y, z) = \frac{S}{2\pi u \sigma_y \sigma_z} \exp \left( -\frac{y^2}{2\sigma_y^2} \right) \left[ \exp \left( -\frac{(z - h)^2}{2\sigma_z^2} \right) + \exp \left( -\frac{(z + h)^2}{2\sigma_z^2} \right) \right]. \quad (6.16)$$

Taking into account dry deposition can be a challenging issue and several approaches exist. The variances,  $\sigma_\star^2$ , are given by parameterizations as a function of

**Fig. 6.4** Ground activity of a radionuclide (in Bq), computed by a Gaussian model (with the Briggs parameterization for  $\sigma_\star^2$ ). Simulation with the POLYPHEMUS system. Credit: Irène Korsakissok, CEREa



the distance to the point source and of the meteorological fields. These (rather) empirical parameterizations can be functions of the atmospheric stability or computed from the meteorological fields (such as the Monin-Obukhov length or the mixing height, Sect. 3.5.2.4).

**Gaussian Puff Model** A natural extension of the Gaussian plume model is the *Gaussian puff model*, that takes into account the time variation of emissions and of meteorological conditions. We suppose that a *puff* is emitted during  $N$  successive time intervals of duration  $\Delta t$ . Each puff has its own evolution, given by a Gaussian model, independently from the others. The resulting concentration is then calculated by summing over all puffs (Fig. 6.5),

$$\forall t \geq N \Delta t,$$

$$C(x, y, z, t) = \frac{1}{(2\pi)^{3/2}} \sum_{i=1}^N \frac{S_i \Delta t}{\sigma_x \sigma_y \sigma_z} \exp \left[ -\frac{(x - x_i(t))^2}{2\sigma_x^2} - \frac{(y - y_i(t))^2}{2\sigma_y^2} \right] \\ \times \left[ \exp \left( -\frac{(z - z_i(t) - h)^2}{2\sigma_z^2} \right) + \exp \left( -\frac{(z - z_i(t) + h)^2}{2\sigma_z^2} \right) \right], \quad (6.17)$$

with  $S_i \Delta t$  the emission at time  $t_i = i \Delta t$ . The location of the puff center  $i$  is given, for instance along the  $x$ -axis, by

$$x_i(t) = x_i(t - \Delta t) + u[x_i(t - \Delta t), t - \Delta t] \Delta t, \quad (6.18)$$

with  $u(x, t)$  the component of the wind velocity along the  $x$ -axis. Modeling the evolution of the puff size is a difficult point for such models: many parameterizations describe the time and space evolutions for  $\sigma_\star^2$  ([10]).

Even if these models have many limitations, they are easy to use, which explains their popularity, especially for applications related to accidental releases of *passive* or *linear* tracers, and to short-range dispersion (Fig. 6.4). Unfortunately, the extension of these models to the reactive case is a challenging issue and lacks rigorous justification.

### 6.1.5.2 Lagrangian Particle Model

A *Lagrangian particle model* is based on the tracking of *numerical particles*. The theoretical background is the stochastic interpretation of the passive dispersion equation (Fokker-Planck equation). For a wind velocity  $\mathbf{V} = (u, v, w)$  and a diagonal diffusion matrix  $K = (K_x, K_y, K_z)$ , the trajectory of a numerical particle is  $(x(t), y(t), z(t))$ . The iteration from time  $t_n$  to time  $t_{n+1} = t_n + \Delta t$  is then

$$x(t_{n+1}) = x(t_n) + \left( u + \frac{\partial K_x}{\partial x} \right) \Delta t + \sqrt{2K_x} \Delta W_x, \\ y(t_{n+1}) = y(t_n) + \left( v + \frac{\partial K_y}{\partial y} \right) \Delta t + \sqrt{2K_y} \Delta W_y, \quad (6.19) \\ z(t_{n+1}) = z(t_n) + \left( w + \frac{\partial K_z}{\partial z} \right) \Delta t + \sqrt{2K_z} \Delta W_z.$$

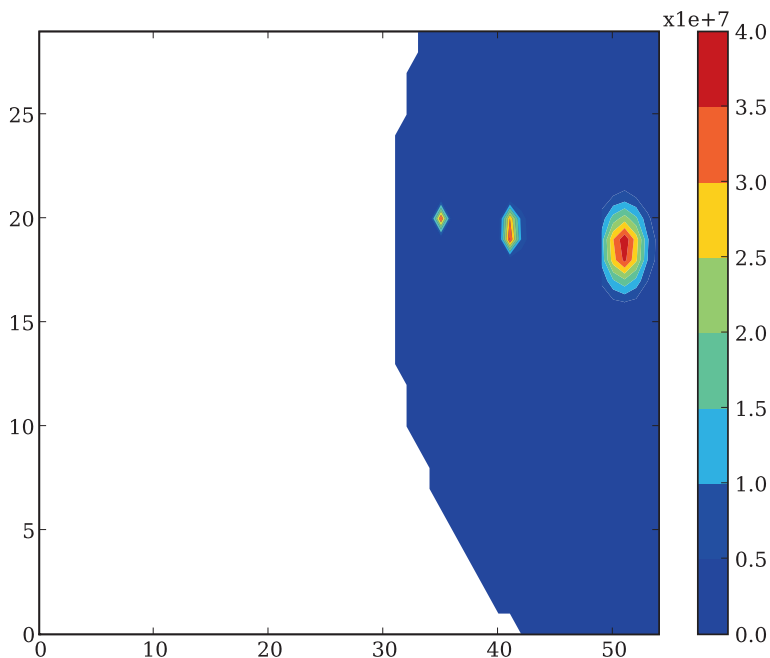


**Fig. 6.5** Ground concentration of an aerosol of diameter  $1\ \mu\text{m}$ , simulated with a puff model. The concentration is dimensionless. Simulation with the POLYPHEMUS system. Credit: Irène Korsakissok, CEREAs

$\Delta W_\star$  is a “white noise”, that is to say a stochastic process following a normal law  $\mathcal{N}(0, \Delta t)$  (with a null mean and a variance  $\Delta t$ ). The resulting concentration  $c$  is calculated by summing over all particles in a given grid cell. It satisfies at the continuous limit (with an infinite number of particles),

$$\frac{\partial c}{\partial t} + \text{div}(Vc) = \text{div}(K\nabla c). \quad (6.20)$$

The advantage of a Lagrangian particle model is a low numerical diffusion, when applied to the dispersion of point sources. The drawback is that the convergence requires a large number of numerical particles (up to tens of thousands). A powerful technique is to use *kernels* by assuming a density to the numerical particles. The extension to the reactive case is however difficult (the correlations between the numerical particles have to be tracked).

### 6.1.5.3 Box Models

The *box models* are defined by considering large domains (“boxes”), as compared to a grid cell, in which the concentrations are supposed to be homogeneous. For an *Eulerian box model*, one gets upon integration of (6.11) and with the boundary

conditions,

$$\frac{d\bar{c}_i}{dt} = \chi_i(\bar{c}) + \frac{1}{z_H}(E_i - v_{dep}^i \bar{c}_i). \tag{6.21}$$

Here, the resolved variable is  $\bar{c} = (\int_0^{z_H} c(z)dz)/z_H$ . We have also assumed that the chemical source term is homogeneous, that is  $(\int_0^{z_H} \chi_i(c(z))dz)/z_H \simeq \chi_i(\bar{c})$ .

Many boxes can be connected by introducing flux terms between boxes. For example, one box can represent the mixing layer ( $z_H$  is then the mixing height, a function of time) while another box can represent the residual layer (Exercise 3.3). These models were very popular in the 1990s but are no longer used.

The *Lagrangian box models* omit turbulent mixing and solve the equations of chemical kinetics (with dry deposition, emissions and wet scavenging) along the characteristic curves of the flow (Exercise 6.4). The computational cost is low, which motivates the use of these models for impact studies in the 1990s (especially for the estimation of source/receptor matrices for transboundary pollution).

6.1.5.4 Chemistry-Transport Models (CTM)

The chemistry-transport models solve (6.11) with appropriate numerical algorithms. The physical parameterizations associated to the different processes are the key components of a CTM. A flow chart is shown in Fig. 6.6.

**Emissions ( $E_i$  and  $S_i$ )** They are usually given by *emission inventories*. The emission inventories are usually poorly accurate. They are based on the so-called *Selected Nomenclature for Air Pollution* (SNAP, Table 6.3 for Greater Paris), defined

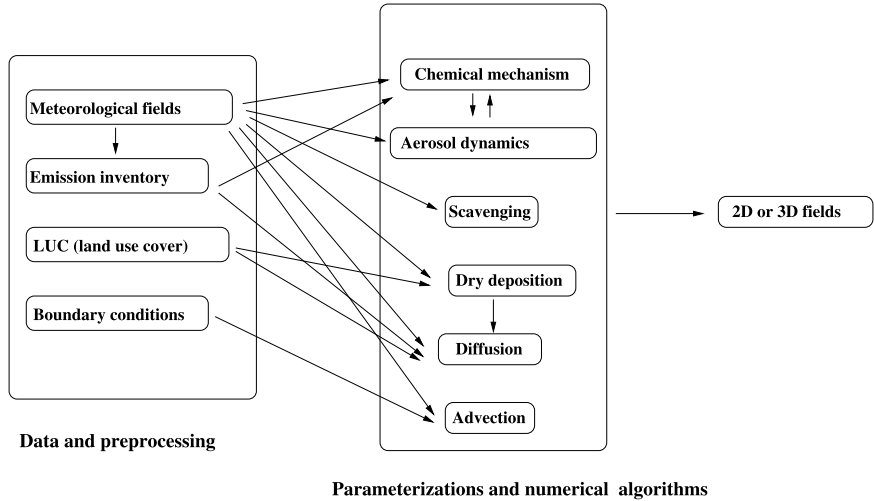


Fig. 6.6 Flow chart of a CTM (off-line coupling)

**Table 6.3** Emission inventory over Greater Paris (Île-de-France, 2006). The total is expressed in  $\text{kt year}^{-1}$  (kt for kiloton); the contribution is in % for each SNAP class. Source: Airparif

	SNAP	$\text{NO}_x$	CO	$\text{SO}_2$	VOCs	$\text{PM}_{10}$	$\text{CO}_2$
1	Energy and urban heating	10	1	40.5	0.5	9	12
2	Residential	12	17	42	7.5	28.5	46
3	Industries	4.5	0	10	0	2	5.5
4	Oil industries	0	0	1	1	18	0
5	Oil distribution	0	0	0	3.5	0	0
6	Solvents	0	0	0	41	0	0
7	Road transport	52	77	3.5	29.5	36.5	29
8	Other mobile sources	9	4	1	2.5	3	3
9	Waste incineration	4.5	1	2.	1	2.5	4.5
10	Agriculture	8	0	0	0	0.5	0
11	Biogenic sources	0	0	0	13.5	0	0
	Total ( $\text{kT year}^{-1}$ )	161	398	68	178	22	49567

as a classification of anthropogenic emissions according to the economic sectors. The time distribution of emissions is often much coarser than the distribution required for a CTM (typically with a resolution of one hour). A challenging issue is to determine the chemical composition of emissions (and the size distribution for primary aerosols). For example, the VOCs are given as a whole. One has first to specify the emissions for the true species (*speciation*) and second to map them for the *model species*, the species actually described in the chemical mechanisms (*aggregation*).

**Meteorological Fields ( $V, T, \rho$ )** The meteorological fields are outputs of the meteorological models. They are mapped onto the CTM meshes. The projection and interpolation steps may be prevailing issues in the preprocessing of a CTM. A specific issue is the so-called *mass consistency* (Exercise 6.7).

**Eddy Diffusion ( $K_z$ )** The parameterization of  $K_z$  is a decisive component of a CTM. Several parameterizations are available: they are functions of the gradients of the potential temperature and of the wind velocity (Chap. 3). A difficult point is the choice of thresholds for  $K_z$  (e.g. its minimal value, typically  $0.5 \text{ m}^2 \text{ s}^{-1}$ ), to be used for the nocturnal boundary layer, characterized by a strong stability (Chap. 3).

**Chemical Mechanisms ( $\chi_i(\cdot)$ )** The chemical mechanism is the second key component of a CTM. For passive tracers or radionuclides, it is replaced by a parameterization of the atmospheric ageing (in practice a lifetime) or by a filiation lifetime. For reactive species the chemical mechanism depends on the targets and on the altitude (see Chap. 4 for a description of tropospheric and stratospheric chemistry of ozone). To date there does not exist any “universal” atmospheric chemical mechanism. A highly detailed mechanism is sometimes referred to as a *master* chemical mechanism. For example, in the case of tropospheric photochemistry, a standard

gas-phase chemical mechanism may describe up to one hundred gas-phase chemical species and a few hundreds of chemical reactions.

**Wet Scavenging ( $\Lambda_i$ )** Scavenging by clouds and precipitations plays a leading role for the soluble gas-phase species and the aerosols (Chap. 5) as it governs their atmospheric residence time. These processes are still poorly known and their parameterization inside three-dimensional models is still a challenging issue. It is all the more difficult that there are large uncertainties in the microphysical parameters that describe rain or clouds.

**Dry Deposition ( $v_i^{dep}$ )** Dry deposition depends on the deposited species, on the meteorological conditions in the surface boundary layer and on the land use cover. It is usually described by a dry deposition velocity (see (6.12)) that is classically parameterized by resistance models (Exercise 3.1). Due to the uncertainties (for instance related to the seasonal evolution of land use coverage), the values of dry deposition velocities are not accurate. Moreover, a few processes, such as codeposition of species, are poorly known.

## 6.2 Fundamentals of Numerical Analysis for Chemistry-Transport Models

This section and the next one present the fundamentals of numerical analysis for chemistry-transport models. The next section investigates the general dynamic equation for aerosols. The content of both sections is quite technical and demands bases in numerical analysis and applied mathematics. A reader interested in the high-level uses of modern simulation systems can omit these sections and should focus on Sect. 6.4 where the numerical model is viewed as a “black box”.

### 6.2.1 Operator Splitting Methods

#### 6.2.1.1 Principle

The reactive dispersion equation can be rewritten in the form

$$\frac{dc}{dt} = \sum_{j=1}^{n_p} f_j(c), \quad (6.22)$$

where  $n_p$  is the number of processes that are taken into account, and  $f_j(c)$  is the source term associated to the process  $j$  (among advection, diffusion, chemical kinetics, etc.). All processes are coupled *a priori* and this equation should be solved by taking into account the  $n_p$  processes simultaneously. In practice, the numerical

methods for solving this equation are usually based on the so-called *operator splitting* method (*operator* stands for process). The principle is to integrate the processes one by one, by solving equations in the form

$$\frac{dc}{dt} = f_j(c). \quad (6.23)$$

There are at least three motivations for splitting:

- appropriate numerical schemes can be applied for each process with tailored properties (see below);
- the computational burden of a coupled approach can be too high (for instance with implicit time integration, see Sect. 6.2.2);
- from a pragmatic viewpoint, such an approach makes it possible to use off-the-shelf submodels, to be plugged into the chemistry-transport model: hence it is easy to modify a parameterization or to add a new process.

Splitting processes that are physically coupled results in errors. The different operator splitting methods aim at reducing the so-called *splitting error*. In case of linear processes ( $f_j(c) = A_j c$  with  $A_j$  a matrix), analytical formulas are available. The splitting error is then easy to estimate in this case.

### 6.2.1.2 A Few Methods

Operator splitting methods are usually presented in the case of two linear processes,

$$\frac{dc}{dt} = A_1 c + A_2 c. \quad (6.24)$$

Let  $c_n$  be the numerical solution computed at time  $t_n$ . The operator splitting method provides a numerical solution  $c_{n+1}$  at time  $t_{n+1} = t_n + \Delta t$  with  $\Delta t$  the so-called *splitting time step*.

**First-Order Splitting** The simplest method is based on a time-integration sequence. For instance, we first integrate  $A_1$  and then  $A_2$  (the sequence can be reversed). The first step is time integration over  $[0, \Delta t]$  of

$$\frac{dc^*}{dt} = A_1 c^*, \quad c(0) = c_n. \quad (6.25)$$

We obtain a solution  $c^*(\Delta t)$ , to be used as an initial condition for the second step. The second step is time integration over  $[0, \Delta t]$  of

$$\frac{dc^{**}}{dt} = A_2 c^{**}, \quad c^{**}(0) = c^*(\Delta t). \quad (6.26)$$

The final solution at  $\Delta t$  provides  $c_{n+1} = c^{**}(\Delta t)$ . It is easy to prove that the *local splitting error* (the error made during one time step) is of second order in  $\Delta t$



(Exercise 6.3). By summing over the global time interval, one gets a *global error* in  $O(\Delta t)$ . Hence this method is said to be a first-order method. We will detail the notions of local and global errors in Sect. 6.2.2.

**Exercise 6.3 (Splitting Error)** Calculate the local splitting error for the first-order method.

**Solution:**

We compare the exact solution  $c(t_{n+1})$  and the numerical solution  $c_{n+1}$ ,

$$c(t_{n+1}) = \exp[(A_1 + A_2)\Delta t]c_n, \quad c_{n+1} = \exp(A_2\Delta t)\exp(A_1\Delta t)c_n,$$

where  $\exp$  stands for the exponential of a matrix. The error is due to the commutation default of matrices:

$$\exp[(A_1 + A_2)\Delta t] = \exp(A_2\Delta t)\exp(A_1\Delta t)$$

is satisfied if and only if  $A_1 A_2 = A_2 A_1$ . We recall the asymptotic expansion  $\exp(A\Delta t) = I + A\Delta t + A^2\Delta t^2/2 + O(\Delta t^3)$  where  $I$  is the identity matrix. It is easy to check that the leading term of the splitting error,  $c(t_{n+1}) - c_{n+1}$ , is  $(A_1 A_2 - A_2 A_1)\Delta t^2/2$ .

Another method is the so-called *source splitting* method. The integration of the first process does not result in a modified initial condition: a source term is added to the contribution of the second process in the second step,

$$\frac{dc^{**}}{dt} = A_2 c^{**} + \frac{c^*(\Delta t) - c_n}{\Delta t}, \quad c^{**}(0) = c_n. \quad (6.27)$$

This method is often advocated when  $A_1$  is a slow process while  $A_2$  includes fast dynamics (Sect. 6.2.1.3).

**Second-Order Splitting** A simple way for reducing the splitting error is to remove the term in  $O(\Delta t^2)$  from the local error splitting. It can be carried out by computing a solution with the sequence  $A_1$ – $A_2$  (let say  $c_{A_1-A_2}$ ) and a second solution with the reversed sequence (let say  $c_{A_2-A_1}$ ). The local error associated to the solution  $(c_{A_1-A_2} + c_{A_2-A_1})/2$  is then of fourth order. This approach requires integration of *four* processes. A more efficient approach is the so-called *Strang splitting*.<sup>1</sup> The symmetry default of the first-order method can be avoided by integrating  $A_1$  over  $[0, \Delta t/2]$ ,  $A_2$  over  $[0, \Delta t]$  and then  $A_1$  over  $[0, \Delta t/2]$ . Each process is thus integrated over a time interval  $[0, \Delta t]$ . The resulting solution is  $c_{n+1} = \exp(A_1\Delta t/2)\exp(A_2\Delta t)\exp(A_1\Delta t/2)c_n$ . It is easy to prove, with an asymptotic expansion, that the local error is of third order with respect to  $\Delta t$ . The method is therefore a second-order method. Note that we have to solve only *three* processes with this algorithm.

---

<sup>1</sup>Named after the American mathematician Gilbert Strang.

### 6.2.1.3 Additional Properties

**Application to the Reactive Dispersion Equation** The error analysis is usually carried out for linear problems. The extension to nonlinear problems is technical and is beyond the scope of this presentation ([81]). Nevertheless, the calculations are easy in the case of an advection-diffusion-reaction equation. We refer to Exercise 6.4 for the case of advection and chemical kinetics. The following theorem summarizes the main results.

**Theorem 6.2.1** *The following pairs of processes have no splitting error:*

- *advection and chemical kinetics if the wind velocity is divergence free and if chemical kinetics does not depend on the spatial location;*
- *diffusion and advection if the wind velocity and the diffusion matrix do not depend on the spatial location;*
- *diffusion and chemical kinetics if the chemical reactions are monomolecular and do not depend on the spatial location.*

Assuming that a process has a weak dependence on the spatial location is *locally* realistic. On the other hand, assuming that the chemical reactions are monomolecular is not possible, except for passive or linear tracers (e.g. radionuclides). The splitting error is then mainly related to the splitting between chemical kinetics and vertical eddy diffusion. Note that the boundary conditions may also induce splitting errors (which is out of the scope of this presentation).

**Exercise 6.4 (Advection-Reaction Model)** We neglect diffusion and we assume that chemical kinetics does not depend on the spatial location. The dispersion model is then

$$\frac{\partial c}{\partial t} + \operatorname{div}(Vc) = \chi(c).$$

We suppose that the wind field is divergence free, namely  $\operatorname{div} V = 0$ . Integrate along the characteristic curves defined by  $dX/dt = V$ . Show that there is no splitting error.

**Solution:**

Let  $\bar{c}(t) = c(X(t), t)$  be the solution along the characteristic curve  $X(t)$ . It is straightforward to obtain

$$\frac{d\bar{c}}{dt} = \frac{\partial c}{\partial t} + \frac{dX}{dt} \frac{\partial c}{\partial x} = \frac{\partial c}{\partial t} + V \frac{\partial c}{\partial x} = \chi(\bar{c}),$$

since  $\operatorname{div}(Vc) = V \cdot \nabla c$  from  $\operatorname{div} V = 0$ . The exact solution can then be computed by splitting: we integrate chemical kinetics along the characteristic curves. This can be interpreted in terms of splitting (the splitting error is null). This result provides the basis for the Lagrangian box models.

**Order Reduction** The error analysis is based on asymptotic expansions with respect to small  $\Delta t$ . In practice, the time step has not a vanishing value: it is typically a few hundreds of seconds for a CTM. A value is “small” only in comparison to

a reference value given by the characteristic timescales of the physical processes. We will see in Sect. 6.2.2 that chemical kinetics is characterized by a wide range of timescales. If  $\tau_f$  is the characteristic timescale of the fastest process, the numerical methods to be used for the time integration of chemical kinetics will be designed so that the numerical timestep is much larger than  $\tau_f$  (otherwise all timescales have to be resolved). Note that the splitting timestep,  $\Delta t$ , is larger than the subcycling timestep used for each process. Hence, we have always  $\Delta t/\tau_f \gg 1$ ! The asymptotic analysis with vanishing values of  $\Delta t$  is then no longer valid. Consequently, the error analysis has to be carried out with another approach. For example, the fastest processes can be filtered out before calculating the local splitting error ([134]). Two results may be retained from this analysis:

- the method order may be reduced: this property is usually referred to as *order reduction* and depends on the characteristic timescales of the species (the fastest species are the most affected ones, as expected);
- the sequence order has an impact when the processes do not have similar characteristic timescales. In practice, advection and diffusion can be viewed as slow processes while chemical kinetics comprises both slow and fast chemical reactions. It is advocated to end the splitting sequence with the fastest processes, so that the system is stabilized.

### 6.2.2 Time Integration of Chemical Kinetics

A key component of a CTM is the time integration of chemical kinetics,

$$\frac{dc}{dt} = \chi(c, T, h\nu), \quad (6.28)$$

where the chemical source term depends on temperature through thermal chemical reactions and on radiation through photolysis reactions. This system of ordinary differential equations (ODEs) is usually characterized by its large dimension (up to one hundred species), by its nonlinear nature (the equations are coupled) and by the wide range of timescales. It is desired to integrate this system of ODE, written in the generic form

$$\frac{dc}{dt} = f(c), \quad c(0) = c_0. \quad (6.29)$$

The time integration algorithms are usually based on an iterative scheme. We suppose that a numerical solution  $(c_k)_{k=1,\dots,n}$  has been computed at times  $(t_k)_{k=1,\dots,n}$  (the subscript  $k$  stands here for time index, not for species). The objective is then to calculate the solution  $c_{n+1}$  at time  $t_{n+1} = t_n + \Delta t$  as a function of the solutions obtained at previous timesteps (possibly only as a function of  $c_n$ ). In this section,  $\Delta t$  stands for the integration timestep of chemical kinetics: it is often referred to as the *subcycling* timestep, with a value lower or equal to the splitting timestep.

### 6.2.2.1 Timescales

For a scalar system  $dc/dt = \lambda c$  (here  $c \in \mathbb{R}$  corresponds to a single species), the solution is  $c(t) = \exp(\lambda t)c(0)$  and the characteristic timescale is  $1/|\lambda|$ . For a linear system,  $dc/dt = Ac$ , with  $c \in \mathbb{R}^{n_s}$  (concentration vector), the characteristic timescales are defined by the inverse values of the Jacobian matrix ( $A$ ) eigenvalues,  $\{\lambda_i\}_i$ . For the sake of clarity, we assume that the Jacobian matrix can be diagonalized in  $\mathbb{R}$  and is nonsingular ( $\lambda_i \neq 0$ ). For a nonlinear system,  $dc/dt = f(c)$ , the linearized system for small perturbations is given by

$$\frac{d(\delta c)}{dt} = \frac{\partial f}{\partial c} \delta c, \quad (6.30)$$

with  $\partial f/\partial c$  the *Jacobian matrix*, often denoted by  $J$ . By extension, the characteristic timescales are *locally* defined by the inverse values of the real parts of the eigenvalues of  $J$ .

### 6.2.2.2 Implicit Schemes Versus Explicit Schemes

**Explicit Schemes** The simplest algorithm is the so-called forward Euler algorithm (or explicit Euler algorithm). The time derivative is approached by a finite difference and the source term is evaluated at time  $t_n$ ,

$$\frac{c_{n+1} - c_n}{\Delta t} = f(c_n), \quad (6.31)$$

which leads to

$$c_{n+1} = c_n + \Delta t f(c_n). \quad (6.32)$$

**Implicit Schemes** In the backward Euler algorithm (also referred to as implicit Euler algorithm), the source term is evaluated at time  $t_{n+1}$ ,

$$\frac{c_{n+1} - c_n}{\Delta t} = f(c_{n+1}). \quad (6.33)$$

It is therefore not possible to compute explicitly  $c_{n+1}$ , given as the implicit solution of an algebraic equation. In case of a linear system, with  $f(c) = Jc$ , it is straightforward to obtain

$$(I - J\Delta t)c_{n+1} = c_n, \quad (6.34)$$

with  $I$  the identity matrix. The solution can be computed once the inversion of the matrix  $I - J\Delta t$  is carried out. In the case of a nonlinear system, an iterative algorithm has to be used in order to solve the algebraic system. For example,  $c_{n+1}$  can be defined as the root of a fixed-point problem,

$$c_{n+1} = g(c_{n+1}), \quad (6.35)$$

with  $g(c) = c_n + \Delta t f(c)$ . The fixed-point algorithm leads to a sequence of iterations labelled by  $k$ , with

$$c_{n+1}^{k+1} = g(c_{n+1}^k) = c_n + \Delta t f(c_{n+1}^k). \quad (6.36)$$

The convergence is reached is  $k$  is large enough, which provides an estimation of  $c_{n+1}$ . When the algorithm is stopped after one iteration, we recover the explicit Euler scheme. An alternative is to use a Newton-like algorithm by rearranging the algebraic equation. The problem is then rewritten in the form

$$g(c_{n+1}) = 0, \quad (6.37)$$

with  $g(c) = c - \Delta t f(c) - c_n$  (we have kept the notation  $g$ ). The Newton algorithm is obtained by linearization, which results in the iterative sequence

$$0 = g(c_{n+1}^{k+1}) \simeq g(c_{n+1}^k) + \frac{\partial g}{\partial c}(c_{n+1}^k)(c_{n+1}^{k+1} - c_{n+1}^k). \quad (6.38)$$

As  $\partial g / \partial c = I - \Delta t \partial f / \partial c$ , we obtain

$$(I - J(c_{n+1}^k) \Delta t)(c_{n+1}^{k+1} - c_{n+1}^k) = -(c_{n+1}^k - \Delta t f(c_{n+1}^k) - c_n), \quad (6.39)$$

with  $J(c_{n+1}^k)$  the Jacobian matrix of  $f$  at point  $c_{n+1}^k$ . Note that this matrix can be approached by  $J(c_n)$  so that the computational cost can be reduced (only the inversion of  $I - J(c_n) \Delta t$  is required). For a fixed time step, an explicit method is always easier to use than an implicit method. The choice of an implicit method is forced by stability constraints.

### 6.2.2.3 Accuracy and Stability

The timestep choice is determined by the error analysis. For a linear system, we can write the previous algorithms in the generic form

$$c_{n+1} = c_n + (1 - \theta) \Delta t f(c_n, t_n) + \theta \Delta t f(c_{n+1}, t_{n+1}), \quad (6.40)$$

with  $\theta$  a numerical parameter in  $[0, 1]$ . If  $\theta = 0$  (1, respectively), we recover the explicit Euler method (the *implicit* Euler method, respectively). The application of this numerical algorithm to the exact solution,  $c(t_n)$ , defines the residual  $\eta_n$  (also referred to as the local truncation error),

$$c(t_{n+1}) = c(t_n) + \Delta t(1 - \theta) f(c(t_n), t_n) + \Delta t \theta f(c(t_{n+1}), t_{n+1}) + \eta_n. \quad (6.41)$$

With a Taylor expansion,

$$\eta_n = \left[ \frac{1}{2}(1 - 2\theta) \frac{d^2 c}{dt^2} \right] \Delta t^2 + O(\Delta t^3), \quad (6.42)$$

where  $d^2c/dt^2 = (\partial f/\partial c) f + \partial f/\partial t$ . A key point is the propagation of this error. Let  $\varepsilon_n = c(t_n) - c_n$  be the *global error* that results from the previous local errors and from their propagations. In the linear case ( $f(c) = \lambda c$ ), we obtain by subtracting (6.40) to (6.41)

$$\varepsilon_{n+1} = \varepsilon_n + (1 - \theta)\lambda\Delta t\varepsilon_n + \theta\lambda\Delta t\varepsilon_{n+1} + \eta_n. \quad (6.43)$$

Let us write  $R(z) = (1 + (1 - \theta)z)/(1 - \theta z)$ . The error propagation is then given by

$$\varepsilon_{n+1} = R(\lambda\Delta t)\varepsilon_n + \delta_n, \quad (6.44)$$

with  $\delta_n = (1 - \theta\lambda\Delta t)^{-1}\eta_n$ . As expected, there are two contributions:

- a *local* contribution (related to the truncation error),  $\delta_n$ , corresponding to the error made in one timestep when the solution at time  $t_n$  is supposed to be exact;
- a contribution corresponding to the error propagation, given by  $R(\lambda\Delta t)$ , which defines the stability property of the algorithm.

With an obvious notation,  $R(z)$  is named the *stability function*. It is a function of the complex variable  $z \in \mathbb{C}$ . Note that the eigenvalues of  $J$  do not have necessarily real values. It is straightforward to obtain

$$\varepsilon_n = [R(\lambda\Delta t)]^n \varepsilon_0 + \sum_{i=0}^{n-1} [R(\lambda\Delta t)]^i \delta_{n-1-i}. \quad (6.45)$$

The stability constraint is supposed to guarantee that the error is bounded. With  $|R(\lambda\Delta t)| < 1$ , we get

$$|\varepsilon_n| \leq |\varepsilon_0| + \sum_{i=0}^{n-1} |\delta_i|. \quad (6.46)$$

Let  $T = n\Delta t$  be the final time. For a local error satisfying  $\delta_i = O(\Delta t^{p+1})$  (here  $p = 1$  or  $p = 2$ ), the global error is controlled by  $n \times O(\Delta t^{p+1}) = T \times O(\Delta t^p)$ . This illustrates the order reduction from the local error to the global error.

#### 6.2.2.4 Stiff Systems

Let us consider dynamical systems that are physically stable (this is the case of atmospheric chemical kinetics): the real part of the eigenvalues of  $J$  are then negative and the linearized system can be written in the form  $dc/dt = -|\lambda|c$ . The stability condition is  $1/(1 + |\lambda\Delta t|) < 1$  for the implicit Euler scheme. This condition is always satisfied and the scheme is said to be *unconditionally stable*. The stability condition is  $|(1 - \lambda\Delta t)| < 1$  for the explicit Euler scheme, namely  $|\lambda\Delta t| \leq 2$ . The choice of the timestep  $\Delta t$  is then constrained by the characteristic timestep so that  $\Delta t \leq 2/|\lambda|$ .

A dynamical system is said to be *stiff* if there is a wide range of characteristic timescales: this means that it comprises both fast processes ( $|\lambda| \gg 1$ ) and slow processes ( $|\lambda| \sim 1$ ). The stability condition is more stringent for the fastest processes: for an explicit scheme, the integration timesteps are then forced to be about the smallest characteristic timescales. In practice, this is not affordable (remember that this corresponds to fractions of seconds for chemical kinetics) and implicit schemes have to be used.

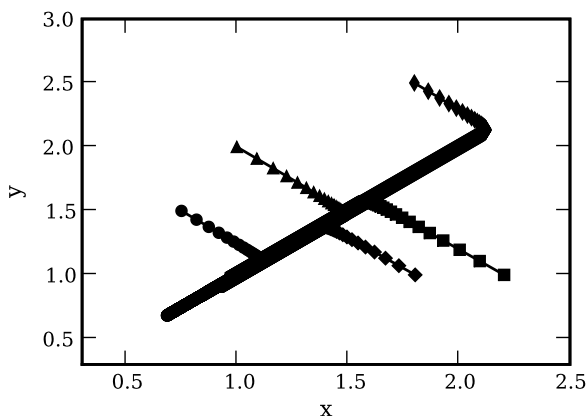
Easy-to-use tailored numerical schemes are still very popular for the time integration of chemical kinetics. Their advantage is that they are simple to implement. Moreover, they are apparently “quicker” than implicit methods since they do not require the inversion of large-dimensional matrices. Note that rigorous analyses, namely by comparing the computational cost against the numerical error (see for instance [125]), have always indicated that these schemes are actually not efficient. We present them for the sake of completeness. Let us consider the loss-consumption form for the time evolution of the concentration of species  $X_i$  (Sect. 4.1.4). The chemical source term is then  $f_i(c) = P_i(c) - L_i(c)c_i$ . The *asymptotic schemes* are based on the linearization of the source term. If  $P_i$  and  $L_i$  are supposed to have constant values over a time interval of length  $\Delta t$ , the solution is

$$c_i^{n+1} = \exp(-L_i^n \Delta t) c_i^n + (1 - \exp(-L_i^n \Delta t)) \frac{P_i^n}{L_i^n}, \quad (6.47)$$

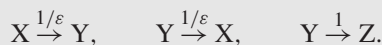
where  $c_i^n = c_i(t_n)$ ,  $c^n = c(t_n)$ ,  $L_i^n = L_i(c^n)$  and  $P_i^n = P_i(c^n)$ . The QSSA scheme (QSSA stands for *Quasi-Steady-State Approximation*, Sect. 4.1.4) is based on the partitioning of species according to their lifetime  $\tau_i^n = (L_i^n)^{-1}$ . For example, for the so-called fast species defined by  $\tau_i^n / \Delta t \ll 1$ , the formula yields  $c_i^{n+1} = P_i^n / L_i^n$ . In practice, there are numerous implementations that may strongly differ. Exercise 6.5 details the theoretical background.

**Exercise 6.5 (Slow/Fast Models)** The wide range of characteristic timescales results in the numerical stiffness. It is deeply associated to the existence of underlying

**Fig. 6.7** Exercise 6.5: convergence of the exact model to the reduced model ( $x = y$ ). The motion along each trajectory is given by the time evolution; each trajectory is defined by an initial condition. The time step between two symbols is constant ( $10^{-3}$ ) along a given trajectory. The timescale ratio is  $\varepsilon = 10^{-2}$



*reduced* models. The simplest example is the chemical mechanism



The values above the reaction arrows correspond to the magnitude of the kinetic rates. The equilibrium between X and Y is characterized by large kinetic rates (of magnitude  $1/\varepsilon$  with  $\varepsilon \simeq 0$ ) while the production of Z is a slow process (with a kinetic rate of magnitude 1). Write the equations for the time evolution of concentrations  $x$  and  $y$  for X and Y. What is the reduced model defined by  $\varepsilon \rightarrow 0$ ? Hint: change the species basis by using  $(u, y)$  with  $u = x + y$  (species *lumping*).

**Solution:**

The time evolution of concentrations is governed by

$$\varepsilon \frac{dx}{dt} = y - x, \quad \varepsilon \frac{dy}{dt} = x - y - \varepsilon y.$$

With the species *lumping*  $u = x + y$ , one gets in the basis  $(u, y)$ ,

$$\frac{du}{dt} = -y, \quad \varepsilon \frac{dy}{dt} = u - 2y - \varepsilon y.$$

For  $\varepsilon \rightarrow 0$ , the evolution equation of  $y$  can be replaced by the algebraic constraint  $y = u/2$ . Hence the system becomes

$$\frac{du}{dt} = -\frac{u}{2}, \quad y = \frac{u}{2}.$$

The underlying model is said to be a *reduced model*. It describes only the time evolution of the slow species (here  $u$ ) while the fast species (here  $y$ ) are supposed to be at equilibrium with the slow species. Note that there is still a time evolution for the fast species but it is not given as such by an evolution equation. All the trajectories, defined by different initial conditions, quickly converge to a reduced model defined by the algebraic constraint  $x = y = u/2$  (Fig. 6.5). A key point is that a change of basis (species lumping) may be required. The asymptotic analysis applied to the initial system would have led to the same algebraic constraint for both species ( $x = y$ , that is  $y = u/2$ ). The reduced system would then have been underdetermined (one equation for two variables).

*To know more* ([136]):

B. SPORTISSE AND R. DJOUAD, *Reduction of chemical kinetics in air pollution modelling*, J. Comp. Phys., **164** (2000), pp. 354–376

### 6.2.3 Advection Schemes

Advection is a key component of a CTM, especially for a passive or linear tracer that is not implied in chemical reactions. The advection equation is

$$\frac{\partial c}{\partial t} + \text{div}(V c) = 0. \quad (6.48)$$



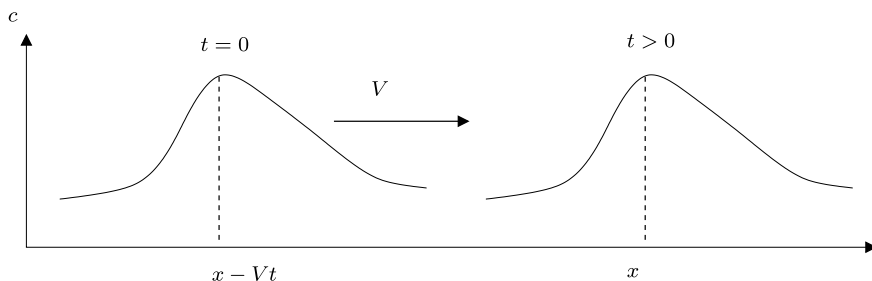


**Fig. 6.8** Tracer advection for a one-dimensional constant wind velocity. The initial concentration distribution is conserved along time

Advection does not couple species and, as a result, we consider only one species. Simulating advection is a challenging issue because a few properties have to be satisfied at the numerical level: mass conservation, positivity of concentrations and monotony (no creation of purely numerical maxima—equivalent to positivity in the linear case).

### 6.2.3.1 Lagrangian and Eulerian Methods

With the *method of characteristics* applied to (6.48), it is straightforward to get the exact solution. Let  $c_0(x)$  be the initial condition. We consider a one-dimensional wind field. It is easy to check that  $c(x, t) = c_0(x - Vt)$  satisfies the advection equation (Fig. 6.8). Similarly, the solution is constant along the so-called *characteristic curves* defined by  $dX/dt = V$ . As  $\bar{c}(t) = c(X(t), t)$ ,

$$\frac{d\bar{c}}{dt} = \frac{\partial c}{\partial t} + \frac{\partial c}{\partial x} \frac{dX}{dt} = 0. \quad (6.49)$$

In the general case ( $V$  is not constant), the most appropriate variable is the mixing ratio  $C$ , whose evolution is governed by  $\partial C/\partial t + V \cdot \nabla C = 0$ . We usually separate the *Lagrangian methods* (and also the *semi-Lagrangian methods*) that are based on this approach, from the *Eulerian methods* that directly solve the PDE by discretization. The drawback of Lagrangian methods is often that they do not satisfy the mass conservation law. We have chosen to focus on Eulerian methods in the following.

### 6.2.3.2 Finite Difference Schemes for Advection

We consider a discretization of the  $x$  axis: let  $(x_i)$  be the resulting nodes with a fixed grid step  $\Delta x$  (Fig. 6.9). We also discretize the time period with the sequence  $(t_n)$ , where the timestep  $\Delta t = t_{n+1} - t_n$  is supposed to have a constant value. For the sake of clarity, the grid and time steps are supposed to be constant. The extension to variable steps is straightforward.

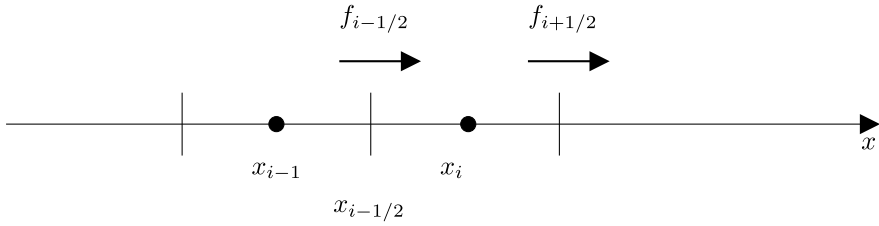


**Fig. 6.9** Finite difference scheme for advection. The flux  $f_{i-1/2}$  is defined at the interface  $x_{i-1/2}$  between the grid cells centered at  $x_{i-1}$  and at  $x_i$

**Spatial Discretization** Let us first introduce the *method of lines*. The principle is first to discretize with respect to space and then to integrate in time the resulting ODE. We use the misleading notation  $c_i(t) \simeq c(x_i, t)$ , where  $i$  corresponds here to the grid cell and not to species (remember that the species are advected one by one).

A *conservative form* of the numerical scheme is

$$\frac{dc_i}{dt} = \frac{f_{i-1/2} - f_{i+1/2}}{\Delta x}, \quad (6.50)$$

where  $f_{i-1/2}$  is a numerical approximation of the flux at  $x_{i-1/2}$ , that is,  $Vc(x - \Delta x/2, t)$ . This form guarantees mass conservation (easy to prove by summing over all cells).

We suppose that  $V > 0$ . The simplest scheme is to approximate the flux by  $f_{i-1/2} = Vc_{i-1}$ . Note that this is equivalent to approximate the spatial gradient by the finite difference  $dc/dx(x) \simeq [c(x) - c(x - \Delta x)]/\Delta x$ . This approach defines the so-called *upwind scheme* (also referred to as the *donor-cell scheme*, with an obvious terminology),

$$\frac{dc_i}{dt} = V \frac{c_{i-1} - c_i}{\Delta x}. \quad (6.51)$$

A second approach is to approximate the flux at  $x_{i-1/2}$  by  $f_{i-1/2} = V(c_{i-1} + c_i)/2$  or, similarly, to use a Taylor expansion for the approximation  $dc/dx(x) \simeq [c(x + \Delta x) - c(x - \Delta x)]/(2\Delta x)$ . The resulting scheme is

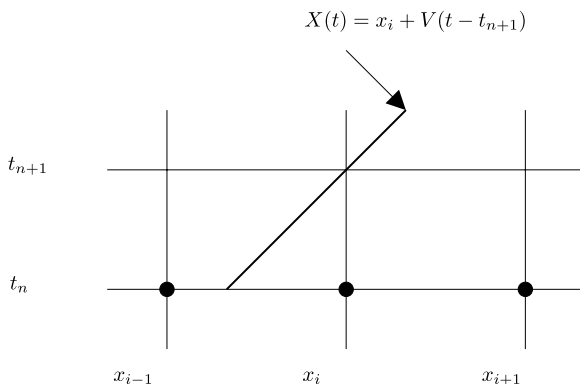
$$\frac{dc_i}{dt} = V \frac{c_{i-1} - c_{i+1}}{2\Delta x}. \quad (6.52)$$

**Time Integration** Let  $c_i^n$  be the numerical solution at time  $t_n$  and at node  $x_i$ . For example, for the upwind scheme, several time integration schemes can be used. The simplest one is the explicit Euler scheme, namely

$$\frac{c_i^{n+1} - c_i^n}{\Delta t} = V \frac{c_{i-1}^n - c_i^n}{\Delta x}. \quad (6.53)$$

Note that this scheme could have been introduced by discretizing simultaneously space and time. This approach is sometimes referred to as the *direct space time*

**Fig. 6.10** Advection schemes and interpolation. Along the characteristic curve defined by  $dX/dt = V$ ,  $c(X(t), t)$  is constant. The black circles indicate the known numerical values at  $t_n$ . Note that  $V\Delta t/\Delta x < 1$  in this case



method. We start from the exact equation satisfied along the characteristic curves

$$c(x_i, t_{n+1}) = c(x_i - V\Delta t, t_n). \quad (6.54)$$

The concentration  $c(x_i - V\Delta t, t_n)$  has then to be interpolated as a function of the computed values ( $c_j^n$ ) at discretization points ( $x_j$ ). For the *upwind* scheme, if  $V > 0$  and  $V\Delta t \leq \Delta x$  (we will comment on this condition below), it is relevant to interpolate the concentration at  $x_i - V\Delta t$  from the values at  $x_{i-1}$  and  $x_i$  (Fig. 6.10). A linear interpolation gives straightforward the upwind scheme written in the form

$$c_i^{n+1} = (1 - a)c_i^n + ac_{i-1}^n, \quad (6.55)$$

with  $a = |V|\Delta t/\Delta x$  the so-called Courant-Friedrichs-Lewy number (CFL).

Note that (6.55) has been obtained with the constraint  $a < 1$ .

### 6.2.3.3 Challenging Issues: CFL Condition, Numerical Diffusion and Mass Consistency

The implementation of the advection numerical schemes faces at least three difficulties:

- the so-called CFL condition,  $a < 1$ , has to be satisfied so that stability is guaranteed;
- the spatial discretization generates numerical diffusion, especially for coarse meshes;
- due to the preprocessed interpolation of the meteorological fields, the mass consistency property may not be met by a CTM.

**Stability and CFL Condition** In a way similar to chemical kinetics (Sect. 6.2.2), the numerical discretization error has two components:

- the local error related to the discretization error for one time step (function of the scheme *order*);

- the propagation of local errors (to be investigated with a *stability* analysis).

The local error is estimated by replacing the numerical solution  $c_i^n$  by the exact solution  $c(x_i, t_n)$  in the iterative scheme. For example, the residual  $\eta_i^n$  of the upwind scheme is

$$\frac{c(x_i, t_{n+1}) - c(x_i, t_n)}{\Delta t} + V \frac{c(x_i, t_n) - c(x_{i-1}, t_n)}{\Delta x} = \eta_i^n. \quad (6.56)$$

Using a Taylor expansion, we obtain  $\eta_i^n = O(\Delta t) + O(\Delta x)$ . Upon subtraction, the global error  $\varepsilon_i^n = c(x_i, t_n) - c_i^n$  satisfies

$$\frac{\varepsilon_i^{n+1} - \varepsilon_i^n}{\Delta t} + V \frac{\varepsilon_i^n - \varepsilon_{i-1}^n}{\Delta x} = \eta_i^n, \quad (6.57)$$

which clearly indicates two contributions. The stability analysis (see also Exercise 6.6) leads to the so-called *Courant-Friedrich-Lewy condition* (CFL condition),

$$a = \frac{|V|\Delta t}{\Delta x} \leq 1. \quad (6.58)$$

Note that this condition is equivalent to the positivity of the solution written in the form (6.55).

The CFL condition can be viewed as a maximal bound for the timestep ( $\Delta t < \Delta x/|V|$ ). Note that the constraint is stringent for high values of wind velocity and for fine meshes. In practice, the CFL condition plays a leading role at the local scale ( $\Delta x \simeq 1$  km in this case, against  $\Delta x \simeq 10$  km at the continental scale).

**Exercise 6.6** (Numerical Diffusion and CFL Condition) This exercise aims at investigating stability and numerical diffusion.

1. We consider a one-dimensional case with a constant wind velocity  $V$ . Using a Taylor expansion of the residual  $\eta$ , prove that the numerical solution computed with the upwind scheme is an approximation of the PDE

$$\frac{\partial c}{\partial t} + V \frac{\partial c}{\partial x} = \frac{V \Delta x}{2} (1 - a) \frac{\partial^2 c}{\partial x^2}.$$

2. This PDE is named the *equivalent PDE* of the upwind scheme: the behavior of the numerical scheme is actually closer to the behavior of the solution to this PDE than to the one of the solution to the advection equation (because the omitted terms are of higher order). Define the *numerical diffusion*. Calculate the numerical diffusion at the continental scale.

**Data:** for horizontal advection,  $V \simeq 5 \text{ m s}^{-1}$ ,  $\Delta x \simeq 10 \text{ km}$ ; for vertical advection,  $V \simeq 0.1 \text{ cm s}^{-1}$ ,  $\Delta x \simeq 50 \text{ m}$ ; in both case,  $\Delta t \simeq 900 \text{ s}$ .

**Solution:**

1. Let us replace  $c_i^n$  by the exact solution  $c(x_i, t_n)$  in the scheme iteration. Using a Taylor expansion up to second order, we obtain

$$\eta_i^n \simeq \left( \frac{\partial c}{\partial t} + V \frac{\partial c}{\partial x} \right) + \frac{1}{2} \left( \Delta t \frac{\partial^2 c}{\partial t^2} - V \Delta x \frac{\partial^2 c}{\partial x^2} \right).$$

The PDE associated with a null residual is the PDE that is the best approximation of the numerical scheme. Up to first order we get the advection equation. There are complementary terms for the second order. If  $\partial c/\partial t + V \partial c/\partial x = 0$ , it is straightforward to check that  $\partial^2 c/\partial t^2 = V^2 \partial^2 c/\partial x^2$  (differentiate  $c$  with respect to  $x$  and then with respect to  $t$ ; reverse the differentiation sequence; equalize the results). If  $\partial c/\partial t + V \partial c/\partial x = \mathcal{O}(\Delta t, \Delta x)$ , this is still valid up to  $\mathcal{O}(\Delta t, \Delta x)$ . Thus, the residual is up to second order

$$\eta_i^n = \left( \frac{\partial c}{\partial t} + V \frac{\partial c}{\partial x} \right) - \underbrace{\frac{V \Delta x}{2} (1-a)}_{K_{num}} \frac{\partial^2 c}{\partial x^2},$$

with  $a = V \Delta t / \Delta x$ . This defines the equivalent PDE.

2. This PDE comprises a diffusion term: let  $K_{num}$  be the numerical diffusion. Note that the numerical diffusion is larger for coarse meshes (large values of  $\Delta x$ ), as expected. Moreover, the stability of a diffusion equation requires the positivity of the diffusion coefficient (otherwise the gradients would grow): hence  $a < 1$  (CFL condition).

At the continental scale, one has for the horizontal advection  $K_{num} \sim 10^4 \text{ m}^2 \text{ s}^{-1}$  and for the vertical advection  $K_{num} \sim 10^{-1} \text{ m}^2 \text{ s}^{-1}$  (to be compared to the values of  $K_z$ , typically ranging from 1 to  $10 \text{ m}^2 \text{ s}^{-1}$ ). The numerical diffusion is then dominant with respect to horizontal diffusion.

**Numerical Diffusion** One of the prevailing issues associated to advection is *numerical diffusion*. Numerical diffusion is actually much larger than horizontal physical diffusion, that is therefore usually neglected. A direct consequence of the interpolation of numerical values along the characteristic curve is to diffuse peaked concentrations over neighboring cells.

Minimizing numerical diffusion is a decisive requirement for applications related to accidental releases of point sources. Indeed, the resulting concentration fields are characterized by strong gradients: there is a polluted plume in a “clean” background (see Fig. 0.7 in Introduction). For photochemistry, the spatial fields are much smoother. Exercise 6.6 presents a powerful approach for the study of numerical diffusion (with the notion of *equivalent PDE*).

**Exercise 6.7 (Mass Consistency)** The objective of this exercise is to introduce a few methods that ensure mass consistency. The simplest numerical approach is the so-called “renormalization technique”.

Let  $c^{n+1} = \mathcal{S}(c^n, V^n)$  be the solution defined by the advection scheme. We assume that the scheme is explicit (this is the case in practice). Let  $\tilde{\rho}^{n+1} = \mathcal{S}(\rho^n, V^n)$  be the air density computed with this scheme: note that this is not the “true” density  $\rho^{n+1}$ , as computed by the meteorological model. Formulate a correction in order to enforce the mass consistency property.

**Solution:**

The correction  $c^{n+1} = (\rho^{n+1} / \tilde{\rho}^{n+1}) \mathcal{S}(c^n, V^n)$  is appropriate. Indeed, if  $c^n = \rho^n$ , we obtain  $c^{n+1} = (\rho^{n+1} / \tilde{\rho}^{n+1}) \mathcal{S}(\rho^n, V^n) = \rho^{n+1}$ . The drawback of this highly simple approach is that artificial mass can be created. Other algorithms have therefore to be used.

*To know more ([138]):*

B. SPORTISSE, D. QUÉLO, AND V. MALLET, *Impact of mass consistency errors for atmospheric dispersion*, Atmos. Env., **41** (2007), pp. 6132–6142

**Off-Line Coupling and Mass Consistency** The mass consistency property was introduced in Exercise 6.1: a passive tracer that is initially well mixed (its mixing ratio is homogeneous) will remain well mixed.

This property is based on the consistency between the wind velocities used for the computation of  $\rho$  and  $c$ , respectively. In practice, for off-line coupling, these two fields are not the same ones: the differences may result from interpolations, from different discretization and from different numerical time integration schemes in the meteorological model (that computes density and wind velocity) and in the CTM (that computes concentrations).

The impact for the numerical simulation of concentrations can be important, especially for accidental releases. The advection process is indeed the leading process in this case. We refer to Exercise 6.7 for a simple approach to satisfy the mass consistency property.

### 6.3 Numerical Simulation of the General Dynamic Equation for Aerosols (GDE)

The numerical simulation of aerosol dynamics (Chap. 5) is the most challenging numerical issue for a CTM. We briefly present the basis of the classical algorithms in this section.

The numerical difficulties are related to the following items:

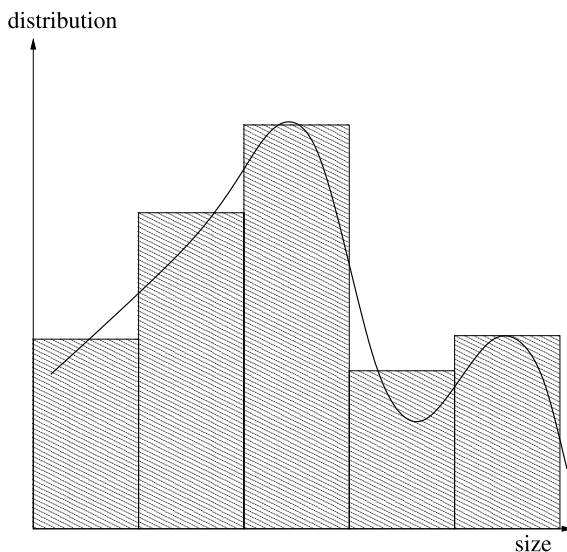
- there is a wide range of time scales and of sizes (for example, the aerosol diameters range from a few nanometers to a few micrometers);
- the resulting models have a large dimension (given by the product of the number of chemical species in the particulate phase by the number of variables used for the description of the size distribution, for a given aerosol family – there is one aerosol family only per single internal mixing);
- the processes that govern the evolution of size distribution and chemical composition are nonlinear; thermodynamics can also be discontinuous (phase transitions, hysteresis phenomena for crystallization and deliquescence of liquid/solid aerosols).

#### 6.3.1 Size Distribution Representation

We can distinguish two different approaches (Fig. 6.11):

- the *modal methods* are based on a decomposition of the size distribution into three or four modes, usually log-normal functions of the diameter (Sect. 5.1, Chap. 5): the variables are then the parameters that describe the modes (distribution moments). Note that the distribution form is fixed *a priori*.
- the *size-resolved methods* that solve the GDE, without any *a priori* form for the distribution.

**Fig. 6.11** Modal description (*curve*) versus sectional description (*gray boxes*: here 5 sections) of an aerosol distribution as a function of a size variable (mass, volume, diameter)



Among the size-resolved methods, we can also distinguish:

- the *sectional methods* (also referred to as *size-binning methods*). They correspond to the application of finite differences algorithms to the GDE: the size distribution is discretized in *sections* (or *bins*) and the numerical variables are related to averaged or integrated quantities over each section.
- the *variational methods*, for which the size distributions are decomposed along basis functions (finite element method or spectral collocation method; Problem 6.1).

We have made the choice of investigating the size-resolved methods because the resulting numerical issues are more challenging than for modal methods. We will also focus on sectional methods (the most classical methods, widely used for their “robustness”).

The aerosol distributions are discretized into a set of *sections* (or *bins*). Let  $n_b$  be the number of sections. The objective is then to calculate  $Q_i^j$  and  $N^j$ , the integrated values over the section  $j$  of the mass distribution function for species  $X_i$  and of the number distribution, respectively.

Coagulation and condensation/evaporation are usually split, which motivates a distinct presentation for each process. Nucleation is easy to solve (a simple source term) and is usually added to condensation/evaporation. Exercise 6.8 illustrates the dynamical behavior of the aerosol processes with the help of simple analytical cases.

**Exercise 6.8** (Analytical Solutions for the GDE) There are analytical solutions for the GDE in a few academic cases.

1. We consider a constant coagulation kernel,  $K_0$ . The size variable is supposed to be the volume,  $v$ . The coagulation equation is therefore

$$\frac{\partial n(v, t)}{\partial t} = \frac{1}{2} K_0 \int_0^v n(u, t) n(v - u, t) du - K_0 n(v, t) \int_0^\infty n(u, t) du.$$

Calculate the evolution of the total aerosol number  $N(t)$ . Comment.

2. We consider the condensation/evaporation equation for the number distribution as a function of the aerosol mass  $m$ ,

$$\frac{\partial n(m, t)}{\partial t} + \frac{\partial [I(m)n(m, t)]}{\partial m} = 0, \quad n(m, 0) = n_0(m).$$

The condensation kernel is supposed to be in the form  $I(m) = \lambda m^{1/3}$  (namely, the growth rate is a linear function of the aerosol diameter). Solve in the case of evaporation ( $\lambda < 0$ ).

Hint: use the variable  $\Psi = I(m)n$  (flux) and then integrate along the characteristic curves defined by the growth rate.

**Solution:**

1. Upon integration of the coagulation equation, we obtain  $dN(t)/dt = -(K_0/2)N^2$  since

$$\int_0^\infty \int_0^v n(v - u, t) n(u, t) du = \left( \int_0^\infty n(u, t) du \right)^2 = N(t)^2.$$

Thus,  $N(t) = N(0)/(1 + t/\tau)$  with  $\tau = 2/(K_0 N(0))$  a characteristic timescale. Note that coagulation results in a decreasing particle number, as expected. In more complicated analytical cases, the Laplace transform can be used to calculate the solutions.

2. The flux  $\Psi$  satisfies

$$\frac{\partial \Psi}{\partial t} = I(m) \frac{\partial n}{\partial t} = -I(m) \frac{\partial \Psi}{\partial m}.$$

The characteristic curves are defined as

$$\frac{d\bar{m}}{dt} = I(\bar{m}) = \lambda \bar{m}^{1/3}, \quad \bar{m}(0) = \bar{m}_0,$$

namely  $(\bar{m})^{2/3}(t) = (\bar{m}_0)^{2/3} + 2\lambda t/3$ . It is easy to check that  $\Psi$  is conserved along the characteristic curves. Thus,  $\bar{m}_0^{1/3} \times n_0(\bar{m}_0) = m^{1/3} \times n(m, t)$  with  $\bar{m}_0$  the initial condition of the characteristic curve with mass  $m$  at time  $t$ . This gives

$$n(m, t) = n_0((m^{2/3} - 2\lambda t/3)^{3/2}) \left( \frac{(m^{2/3} - 2\lambda t/3)^{3/2}}{m} \right)^{1/3}.$$

The calculation is more complicated in the case of condensation because it requires a boundary condition at  $m = 0$  (in practice given by the nucleation rate).



### 6.3.2 Coagulation

**Partitioning Coefficients** For the sake of clarity, we focus on the coagulation equation for the number distribution (the so-called Smoluchowski equation, [149]). Upon integration of (5.7) (Chap. 5), we obtain

$$\frac{dN^j}{dt}(t) = \frac{1}{2} \sum_{j_1=1}^j \sum_{j_2=1}^j X_{j_1 j_2}^j N^{j_1} N^{j_2} - N^j \sum_{j_1=1}^{n_b} X_{j j_1} N^{j_1}. \quad (6.59)$$

The coefficients  $X_{j_1 j_2}^j$  are the key components of the sectional methods for coagulation. They describe the fraction of aerosols that are in section  $j$ , and that result from the coagulation of sections  $j_1$  and  $j_2$ , (Fig. 6.12).  $X_{j_1 j_2}^j$  is defined by summing over all sections:  $X_{j_1 j_2}^j = \sum_{j=1}^{n_b} X_{j_1 j_2}^j$ .

We refer to [33] for a synthesis of the existing methods and a rigorous justification (the methods are usually rather empirical). A key point is the closure scheme used to form the distribution function inside each section.

**Time Integration** In a second step, the resulting system of ODE is integrated with a time integration scheme. There are no specific numerical difficulties and explicit methods can be used.

### 6.3.3 Condensation and Evaporation

The condensation/evaporation equation corresponds to a hyperbolic problem, similar to the advection equation (the spatial coordinates are replaced by size variables). The numerical simulation of this process is the most challenging step for the GDE because there is a wide range of timescales (condensation onto the fine aerosols is a fast process, Exercise 6.9).

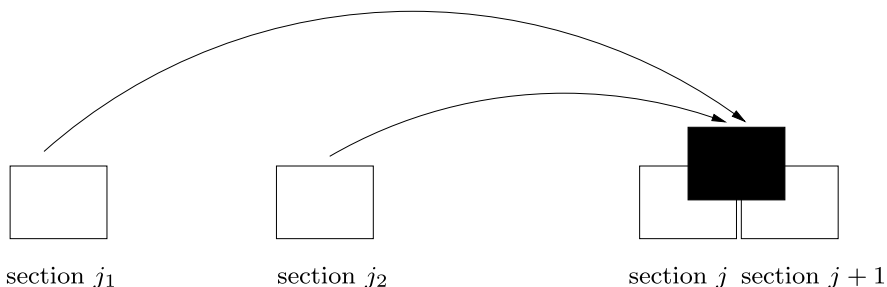


**Fig. 6.12** Coagulation of aerosols from sections  $j_1$  and  $j_2$ . The resulting aerosols (in black) have to be partitioned among the fixed sections that define the discretization of the size distribution functions

As for advection, we can distinguish two numerical approaches:

- the Eulerian methods are based on a *fixed* discretization of the size distribution; the mass transfer fluxes have to be computed at the interface between sections.
- the growth of a given section is tracked in Lagrangian methods.

Due to the rather low number of affordable sections in a three-dimensional CTM, the Eulerian methods are usually not advocated because they may result in a large numerical diffusion (see Exercise 6.6). Hence, we focus on Lagrangian methods.

A popular method is the so-called *moving sectional algorithm* ([66, 75]), that can be interpreted as a Lagrangian approach with specific numerical tricks. A difficult issue is the mapping of the (calculated) Lagrangian distribution onto the fixed sections required for the transport of aerosols inside a CTM.

From the definition of the growth rate in (5.15) (Chap. 5), we obtain a system of EDOs that gives the time evolution of the Lagrangian variables, for example the mass distributions for the  $n_s$  chemical species in the particulate phase,

$$\frac{dQ_i^j}{dt} = N^j I_i(Q_1^j, \dots, Q_{n_s}^j), \quad (6.60)$$

where  $i$  labels chemical species and  $j$  sections.

The growth rate depends on all the chemical species through the thermodynamic equilibrium at the aerosol surface. Solving the equilibrium conditions is a difficult point, which results in a heavy computational burden in the computation of  $I_i$ : as a result, the computational cost of a multiphase CTM is mainly related to the computational cost of the thermodynamic module for aerosols.

This system of EDOs is stiff due to the wide range of timescales associated with the different aerosol sizes (Exercise 6.9). Using implicit methods is not necessarily appropriate because the calculation of the Jacobian matrix may be not affordable (this would require a large number of calls to the thermodynamic module). An alternative approach is based on the so-called *hybrid methods*. Similar to the QSSA methods used for chemical kinetics, the fast part of the aerosol variables (namely the variables related to the finest aerosols) are supposed to be at equilibrium while the dynamic mass transfer is solved for the slow part (the variables associated to the remaining part of the aerosol distribution). Note that an explicit solver can then be used (the fast dynamics have been removed).

**Exercise 6.9** (Characteristic Timescales for Condensation) Equation (5.19) of Chap. 5 defines the growth rate. Estimate the magnitude of the resulting characteristic timescales as a function of the aerosol size.

**Solution:**

For a given chemical composition,  $I_i(d_p) \sim d_p \times f(K_n, \alpha)$ . If  $K_n \gg 1$ , this yields  $I_i(d_p) \sim d_p^2$ , while if  $K_n \ll 1$ ,  $I_i(d_p) \sim d_p$ . We define an approximated timescale by  $\tau \simeq m_i(d_p)/I_i$  with  $m_i(d_p)$  the mass of species  $X_i$  inside aerosols of diameter  $d_p$ . As  $m_i(d_p) \sim d_p^3$ , we obtain  $\tau \sim d_p$  for  $K_n \gg 1$ , and  $\tau \sim d_p^2$  for  $K_n \ll 1$ . Mass transfer is therefore very fast for the finest aerosols, which quickly reach the thermodynamic equilibrium.

*To know more ([31]):*

E. DEBRY AND B. SPORTISSE, *Reduction of the condensation/evaporation dynamics for atmospheric aerosols: theoretical and numerical investigation of hybrid methods*, J. Aerosol Sci., **37** (2006), pp. 950–966

## 6.4 State-of-the-Art Modeling System

### 6.4.1 Forward Simulation

From now on, the CTM is supposed to be built, which means that the physical parameterizations and the numerical algorithms have been chosen. The CTM can be envisioned as an input/output function (a “black box”): the outputs  $y$  (concentrations, deposition fluxes, etc.) are computed from the inputs  $x$  (parameterization data, initial conditions, boundary conditions, etc.) with

$$y = F(x). \quad (6.61)$$

This defines the so-called *forward mode* of the CTM: for a given input  $x$ , we compute the output  $y$ .

### 6.4.2 Uncertainties

If the inputs were accurate (that is to say, if the physical parameterizations and the numerical algorithms were accurate), it could be sufficient to use the CTM only in the forward mode. In practice, the CTMs are characterized by many uncertainties (Table 6.4):

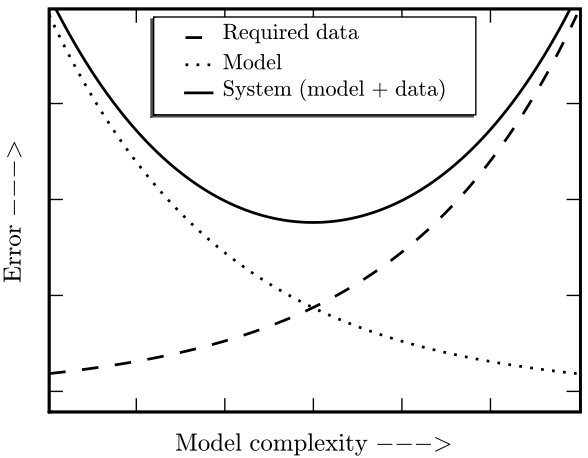
- the input data have often a poor accuracy (a limiting step is the quality of the inventory emissions);
- the meteorological fields have their own uncertainties, which will affect in turn the CTM;
- the subgrid parameterizations (related to the wide range of spatial scales) induce errors that are usually not controlled;
- due to the large dimension, the numerical discretization is often coarse (especially for aerosol dynamics);
- the software systems also contain bugs.

More and more complicated processes should be included in a CTM (especially due to model couplings), which requires the use of finer and finer data, that are usually poorly accurate. Formally, the ideal modeling system is characterized by a trade-off between the data quality and the model complexity (Fig. 6.13). Note that the data are related not only to the input data but also to the observational data, to be used for the model validation and for data assimilation (see below).

**Table 6.4** Typical uncertainties of the CTM inputs at the regional scale. Source: [51]

Data	Relative uncertainties
Cloud attenuation	±30%
Dry deposition velocity (O <sub>3</sub> and NO <sub>2</sub> )	±30%
Boundary conditions (O <sub>3</sub> )	±20%
Anthropogenic emissions	±50%
Biogenic emissions	±100%
Photolysis rate	±30%

**Fig. 6.13** Evolution of model errors and of data errors as a function of the model complexity (resolution). A complicated model is accurate but it requires the use of highly detailed data (that are therefore uncertain in practice); a simple model is poorly accurate but it requires easy-to-obtain data (usually accurate). The global error is evaluated by summing the model error and the data error



6.4.3 Advanced Methods

6.4.3.1 Sensitivity Analysis

We consider a scalar input with continuous values, typically a parameter used in a parameterization or a component of initial or boundary conditions. The uncertainties can be evaluated by sensitivity analysis. The principle is to compute the vector of partial derivatives of outputs with respect to the input data,

$$s = \frac{\partial F}{\partial x}. \tag{6.62}$$

The model associated to  $\partial F/\partial x$  is usually referred to as the *linear tangent model*. For a *small* perturbation applied to a scalar input data  $x$  (say  $\delta x \in \mathbb{R}$ ), we can calculate the propagation resulting in the outputs,  $s\delta x$ . For a nonlinear model, this approximation is only valid in the vicinity of the value  $x$  at which the partial derivative is computed.

Similarly, it may be useful to search for the impact of perturbations applied to a *set* of input data on a given scalar output. For example, the sensitivity of the mean mercury concentration with respect to the mercury emissions is shown in Fig. 6.14.

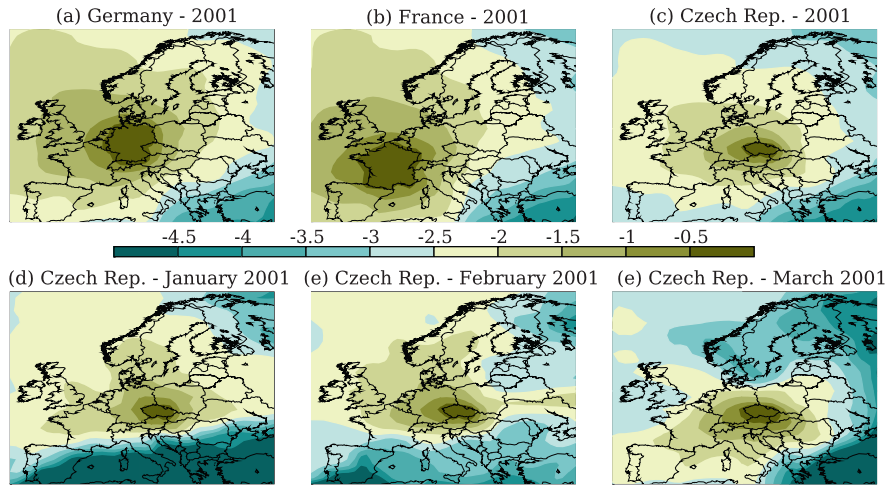


**Fig. 6.14** Map of the sensitivity ( $\log_{10}$ -scale) of the ground averaged mercury concentration with respect to the mercury emissions. The averaged concentration is computed for a given domain and over a given time interval that are indicated for each case. Credit: Yelva Roustan and Marc Bocquet, CEREIA. Source: [123]

The computations are carried out with the so-called *adjoint model* (Problem 6.2). Such studies are of course relevant to investigate transboundary pollution: the objective is indeed to express the dependence of targets on emissions. A source/receptor matrix can be generated from the sensitivity coefficients  $\partial F/\partial x$ , with  $F$  the concentration vector (or the vector of deposition fluxes) and  $x$  the emission vector.

#### 6.4.3.2 Monte Carlo Methods

Monte Carlo methods are widely used in order to evaluate the global uncertainties in a continuous parameter. Let  $P(x)$  be the *probability density function* (PDF) of the uncertain input  $x$ . The averaged output value is approached by  $\langle y \rangle = \int P(x)dx$  with a sampling of  $x$  by  $N$  values  $(x_i)_i$ ,

$$\langle y \rangle \simeq \frac{1}{N} \sum_{i=1}^N F(x_i). \quad (6.63)$$

More generally, we can compute the PDF associated to  $y$  (Fig. 6.15). The convergence rate can be estimated by  $\text{Var}(y)/\sqrt{N}$  with  $\text{Var}(y)$  the variance of  $y$ , to be viewed as a random variable. As a result, a large number of sampling points have to be computed. The convergence is thus rather slow (even if variance reduction methods can be used in order to quicken the convergence).

**Fig. 6.15** Evolution of the PDF associated to the averaged values of ozone (over one day) over Europe (summer 2001). The PDF is computed by a Monte Carlo method applied to a set of continuous input parameters (with  $N = 800$  simulations). Simulation with the POLYPHEMUS system; credit: Vivien Mallet, CERE

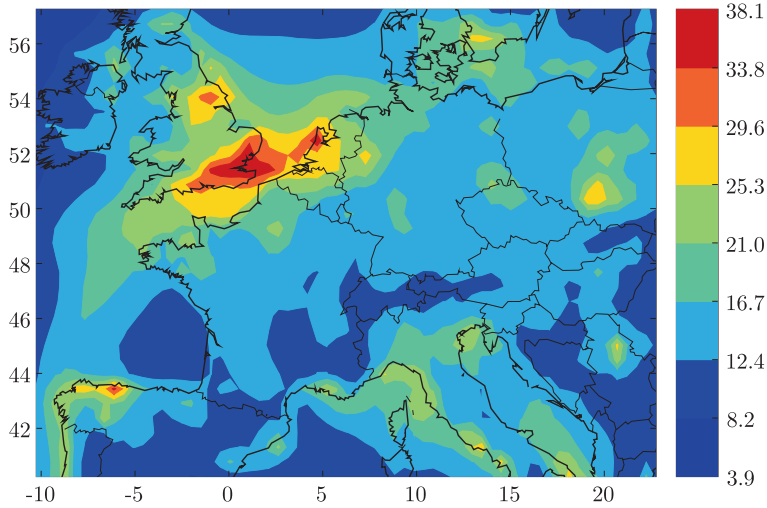
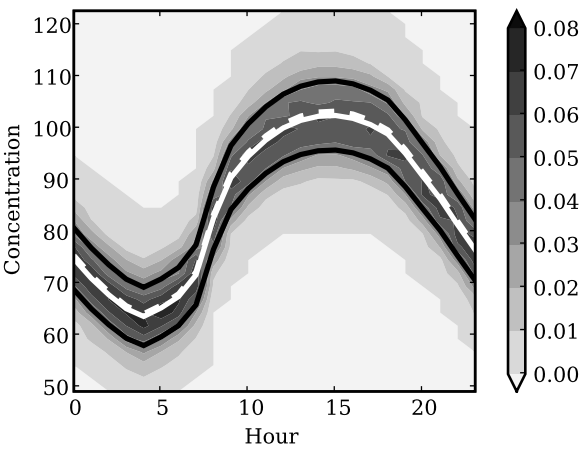


**Fig. 6.16** Variance for the ozone concentration (relative uncertainty, in %) in a multi-model configuration of the POLYPHEMUS system (summer 2001). An ensemble of 48 model configurations is used. Credit: Vivien Mallet, CERE

### 6.4.3.3 Ensemble Simulation: Multi-Model Ensemble

In practice, there exist a few alternative parameterizations for a given process. There is no *a priori* motivation for selecting one parameterization rather than another. The parameterizations can generate different inputs  $(x_i)_i$  or define different model configurations  $(F_i)_i$ .

A multi-model system is able to provide an *ensemble* of outputs,  $(F(x_i))_i$ ,  $(F_i(x))_i$  or  $(F_i(x_j))_{i,j}$ . This gives an estimation of the spread in the outputs and of the uncertainty propagation (Fig. 6.16).

### 6.4.3.4 Ensemble Forecast

For forecast purposes, it is desired to estimate not only the uncertainties but also the best available concentrations. *Ensemble forecast methods* are combinations of  $N$  model outputs, written as  $(y_i)_{i=1, N}$  (Fig. 6.17). Many approaches can be used.

- The simplest method is the *ensemble mean* with  $y = (\sum_{i=1}^N y_i)/N$ .
- For applications related to accidental releases, the median value (chosen among the outputs ranked in increasing order) is often used.
- A more sophisticated and more rigorous approach is based on a linear combination of the model outputs,

$$y = \sum_{i=1}^N \alpha_i y_i. \quad (6.64)$$

The weighting vector  $\alpha$  is estimated by comparing the resulting forecast with the available observations: this can be performed by minimizing the cost function that accounts for a deviation from the past observations (the function is not detailed here). The ensemble forecast will favor the “good” models, to be selected when more and more observations become available. Such methods can dramatically improve the forecast quality, especially for photochemistry. They can also be viewed as examples of data assimilation techniques (see next section).

*To know more ([91]):*

V. MALLET AND B. SPORTISSE, *Ensemble-based air quality forecasts: a multi-model approach applied to ozone*, J. Geophys. Res., **111** (2006), p. 18302

### 6.4.3.5 Data Assimilation and Inverse Modeling

**Background** The current state-of-the-art modeling systems include *data assimilation* procedures. Indeed, there are other information sources next to the numerical

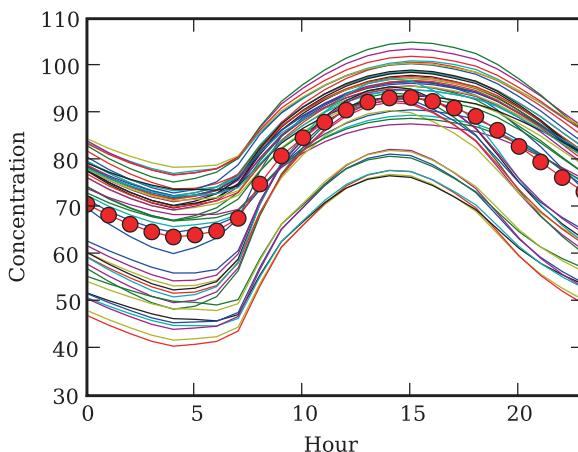


**Fig. 6.17** *Ensemble simulation of ozone with 48 models. Computed with the POLYPHEMUS system (averaged daily evolution, summer 2001). The red points stand for the ensemble mean. Credit: Vivien Mallet, CEREIA*

models: monitoring networks provide observational data. The monitoring networks can be ground networks devoted to air quality, satellite sensors devoted to observation of the atmospheric composition or wifi urban networks in the near-future (with thousands of sensors).

A data assimilation method enables coupling between models and observations. It can be interpreted as the application to the model outputs of a constraint provided by observational data. Similarly, it can be viewed as an interpolation of measurements (that do not give complete information: there are not enough sensors) under the model constraints (that respect physical laws). Exercise 6.10 illustrates the most basic algorithm, namely the so-called optimal interpolation method.

**Exercise 6.10 (Optimal Interpolation Method)** Let  $y_m$  and  $obs$  be the values computed by the model and given by the observations, respectively. Both values are uncertain: we write  $\sigma_m^2$  and  $\sigma_o^2$  the estimated variances, for  $y_m$  and  $obs$  respectively. Thus,  $1/\sigma_\star^2$  can be interpreted as the confidence given to the value under consideration. In order to estimate the concentration  $y$ , we want to minimize the *cost function*  $J$ ,

$$J(y) = \frac{1}{2\sigma_m^2}(y - y_m)^2 + \frac{1}{2\sigma_o^2}(y - obs)^2.$$

$J$  describes the discrepancy between both information sources, weighted by their confidence. Estimate the so-called *analysis*,  $y_a$ , defined as the value that realizes the minimum of  $J$ . Comment.

**Solution:**

$J$  is a convex function whose minimum satisfies  $\partial J / \partial y = 0$ , namely

$$y_a = \frac{\frac{y_m}{\sigma_m^2} + \frac{obs}{\sigma_o^2}}{\frac{1}{\sigma_m^2} + \frac{1}{\sigma_o^2}}.$$

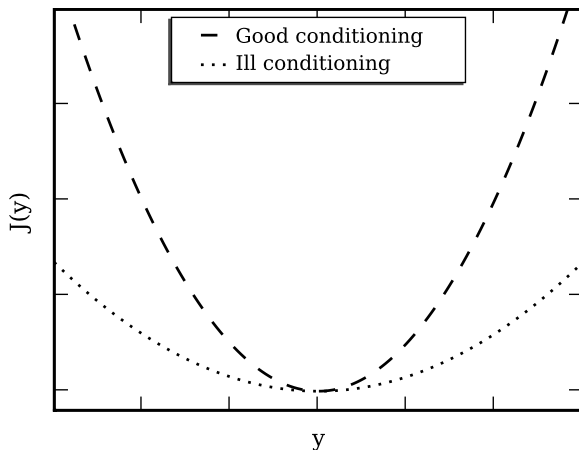
It is straightforward to comment on the resulting analysis for different magnitudes of the variances. Moreover, this approach has a probabilistic interpretation (not detailed here). Note that the solution quality is given by the ability to compute a minimum of  $J$ : when the minimum is “flat”, the solution quality is weak (Fig. 6.18). Note that the method requires inversion of the Hessian matrix of  $J$ .

**Inverse Modeling** A similar application is provided by *inverse modeling* (also referred to as *parameter identification*). The objective is then to estimate an *uncertain* input parameter. The typical example is the inverse modeling of emission fluxes in order to lower the uncertainties of an emission inventory. Other applications are to check that a commitment to emission reduction is met, or to localize sources of accidental releases that are detected by a monitoring network.

The simplest case is the linear case  $y = Ax$ , where  $x \in \mathbb{R}^p$  corresponds to the input data. Let  $H$  be the *observation operator*, supposed to provide observations  $obs = Hy$ , defined as a linear function of the state vector  $y$ . For a ground sensor,  $H$  is associated to time and space sampling for the measurements of a given chemical



**Fig. 6.18** Conditioning of the cost function  $J$  with respect to inversion. The conditioning is related to the properties of the Hessian matrix of  $J$  (second derivative)



species. It is usually not possible to measure all the components of the state vector and  $obs \in \mathbb{R}^m$  with  $m \ll p$ .

In case  $m = p$  and when there is no observational error, we obtain  $obs = HAx$ : the inversion of this linear algebraic system would give a value for  $x$ . In practice, the system is underdetermined and the observational errors have to be taken into account. Let  $x_b$  be so-called *background* value for  $x$ : it is a first guess of the true value. Similarly to data assimilation, the solution is given by the minimization of the cost function

$$J(x) = \frac{1}{2}(obs - HAx)^T R^{-1}(obs - HAx) + \frac{1}{2}(x - x_b)^T B^{-1}(x - x_b), \quad (6.65)$$

where  $R$  and  $B$  stand for the error covariance matrices for the observation and the background, respectively. For example,  $R$  may be a diagonal matrix with coefficients  $\sigma_o^2$ . The transpose vector of the vector  $M$  is  $M^T$ .

This method is usually referred to as the *3D-Var method*; “3D” refers to the fact that only space is taken into account (see below for time).

Such methods are used for the inversion of methane emissions (for example [14]), of CO ([23] at the regional scale, [13] at the global scale), of  $NO_x$  ([116], Fig. 6.20), of volatile organic compounds ([22]), etc. In the case of accidental releases, we have usually to deal with point-source emissions, contrary to the previous cases (diffuse emissions). A related issue may be the *localization problem* (see for instance Fig. 6.21), especially for radionuclides.

In the future, numerical models will be increasingly used for such applications.

**Time Evolution** This framework can be generalized to the case of time-dependent systems. Let  $(obs_i)_i$  and  $(y(t_i))_i$  be the sequence of observed values and of computed values at times  $(t_i)_i$ , respectively. We write  $H_i$ , the observation operator at time  $t_i$ , that maps the simulated values to the observations.

We usually split the *sequential methods*, based on estimation theory (Kalman filtering, Fig. 6.19), from the *variational methods*, based on minimization of the

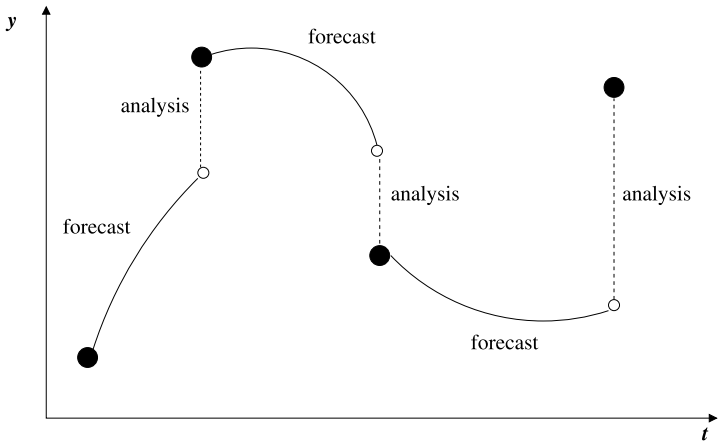


**Fig. 6.19** Data assimilation with a sequential method. When an observation is available, the *analysis* is computed so that the state is corrected (with a method similar to Exercise 6.10). The analysis is thereafter used as the initial condition for the model forecast

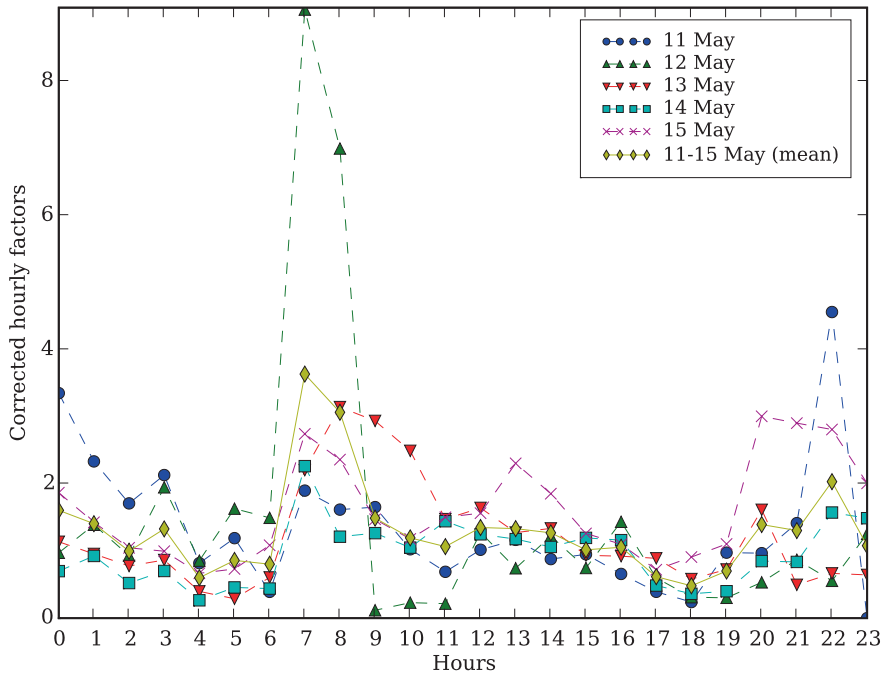


**Fig. 6.20** Correction of the hourly emission factors for  $\text{NO}_x$  with inverse modeling (air quality simulation over Lille in northern France). In the reference emission inventory, the factor is equal to 1. Source: [116]

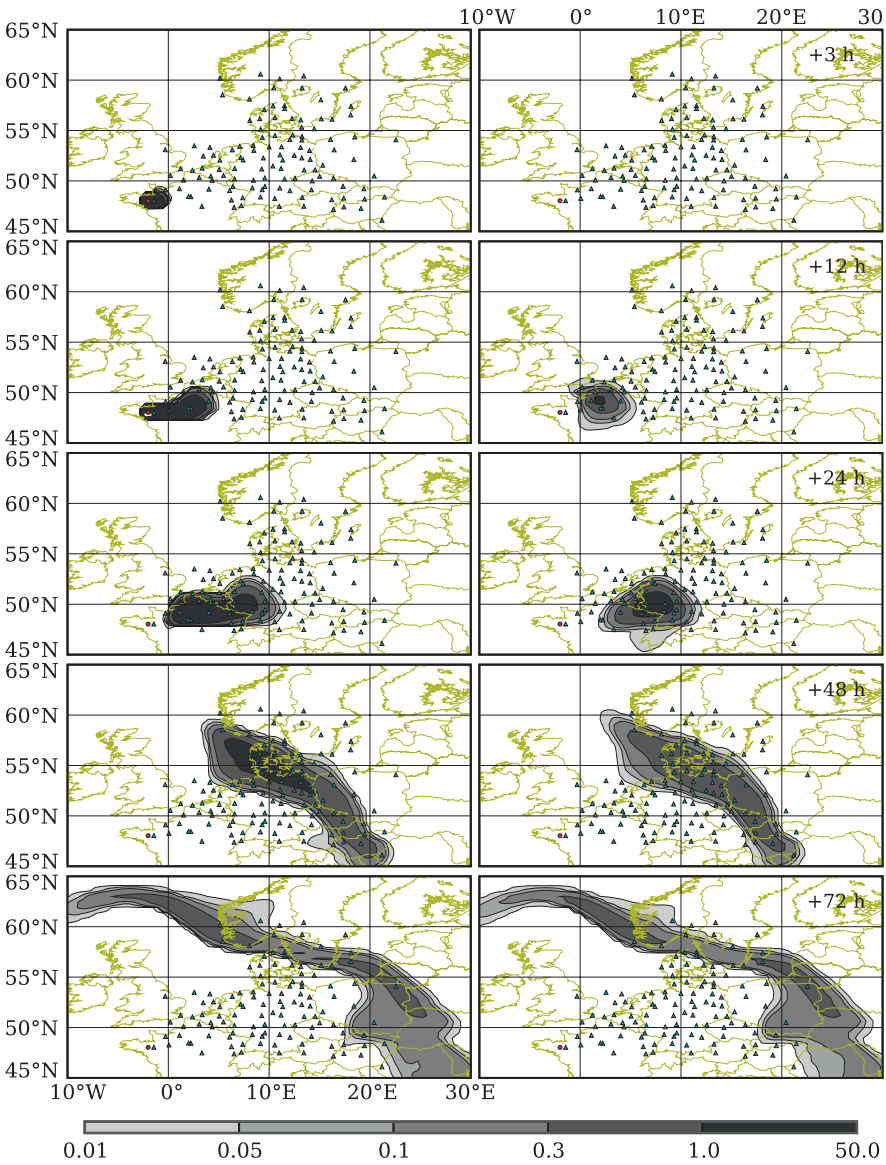


**Fig. 6.21** Source reconstruction from the observational data given by a monitoring network, and the resulting forecast of the pollutant dispersion. The observational data are issued from the ETEX campaign (*European Tracer EXperiment*, 1994, [101]): a tracer was emitted near Rennes (in Brittany, France). *Left*: plume simulation with the true emission. *Right*: plume simulation after source reconstruction from the real-time measured data (stations indicated by triangles). In this case, about ten hours of observation are required for localizing the emission source. The unit is  $\text{ng m}^{-3}$ . Credit: Marc Bocquet, CEREAs. Source: [15]

cost function over a time interval (an ensemble of observations is taken into account simultaneously).

For example, the parameter to be controlled may be the emission flux  $x$ . We assume that the numerical model provides a sequence of values  $y(t_{i+1}) = F(y(t_i), x)$ . A variational formulation (defining the *4D-Var method*) is based on the minimization of the cost function

$$J(x) = \frac{1}{2} \sum_{i=1}^n [\text{obs}_i - H_i y(t_i)]^T R_i^{-1} [\text{obs}_i - H_i y(t_i)] + \frac{1}{2} (x - x_b)^T B^{-1} (x - x_b), \quad (6.66)$$

where the notations are coherent with the previous cases. The key point is that the sequence of simulated values ( $y_i$ ) is constrained by the numerical model and depends on  $x$ . The cost function  $J(x)$  is usually minimized with a gradient-like method. The simplest method is to calculate a sequence  $x^{k+1} = x^k - \alpha_k \nabla_x J(x^k)$  ( $\alpha_k > 0$  is a numerical parameter): the solution is then obtained after convergence (for  $k$  large enough).

The computation of  $\nabla_x J$  is unfortunately a challenging issue, as compared to the case of optimal interpolation (Exercise 6.10). We refer to Problem 6.2 for the introduction of a powerful method, based on the so-called *adjoint model*.

### 6.4.4 Model-to-Data Comparisons

The numerical models are extensively compared to observational data, which should be chosen as various as possible (spatial areas, time periods, chemical or radiative outputs; ground stations, vertical profiles, airborne sensors, satellite data). Notice that it is more relevant to refer to model-to-data comparisons rather than to model *validation*. For example, there are only a limited number of observed chemical species: aerosols are usually measured through a bulk mass ( $\text{PM}_{10}$ ); most of the observations are at ground (while the fields are three-dimensional fields) and are not necessarily well sampled (Fig. 6.22), etc.

The evaluation of a model performance has been strictly defined, especially by the US EPA (*Environmental Protection Agency*). Statistical indicators are used, depending on the targets and on the application:

- for an accidental release (point-source emission of a pollutant not supposed to be in the atmosphere), the indicators will focus on the model's ability to forecast the *arrival times* of the pollutant plume or the maximum values.
- for photochemistry, the concentration fields are much more diffuse and numerous observational data may be available. The classical indicators are based on statistical criteria (Table 6.5). For example, the recommendations of the US EPA focus on the limit values for the so-called MNBE (at  $\pm 5\%$ ), MNGE (at  $\pm 30\%$ ) and UPA (at  $\pm 15\%$ ) for ozone concentrations that are not above a given threshold (typically from 40 to 60 ppb). Note that the results can be highly sensitive to the choice of the monitoring network (Table 6.6 and Table 6.7). A key point is the *representativity* of a monitoring station: actually, a point measurement has to be compared with a numerical output, *averaged* over a grid cell.

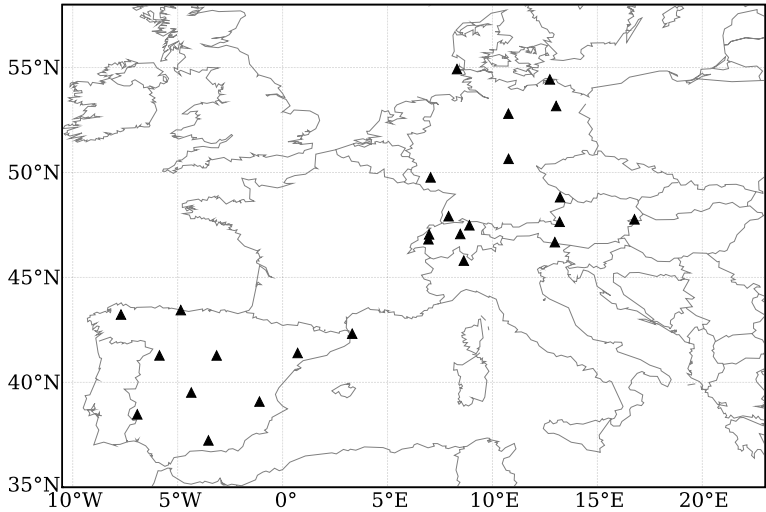


**Fig. 6.22** Localization of the EMEP stations for PM<sub>10</sub>. Credit: Yelva Roustan, CERE

**Table 6.5** A few statistical indicators to compare observed and simulated time sequences with  $n$  elements. The simulated values are  $(y_i)$  while the corresponding observational data are  $(obs_i)$ . The averaged value for the field  $\Psi$  is denoted as  $\overline{\Psi}$ . Source: [124]

Indicator	Notation	Formula
Root Mean Square Error	RMSE	$\sqrt{\frac{1}{n} \sum_{i=1}^n (y_i - obs_i)^2}$
Bias	Bias	$\frac{1}{n} \sum_{i=1}^n (y_i - obs_i)$
Mean Fractional Bias	MFB	$\frac{1}{n} \sum_{i=1}^n \frac{(y_i - obs_i)}{(y_i + obs_i)/2}$
Mean Fractional Error	MFE	$\frac{1}{n} \sum_{i=1}^n \frac{ y_i - obs_i }{(y_i + obs_i)/2}$
Correlation	Corr	$\frac{\sum_{i=1}^n (y_i - \overline{y})(obs_i - \overline{obs})}{\sqrt{(\sum_{i=1}^n (y_i - \overline{y})^2) (\sum_{i=1}^n (obs_i - \overline{obs})^2)}}$
Mean Normalized Bias Error	MNBE	$\frac{1}{n} \sum_{i=1}^n \frac{y_i - obs_i}{obs_i}$
Mean Normalized Gross Error	MNGE	$\frac{1}{n} \sum_{i=1}^n \frac{ y_i - obs_i }{obs_i}$
Unpaired Peak Prediction Accuracy	UPA	$\frac{y_{max} - obs_{max}}{obs_{max}}$

6.4.5 Applications

The air quality numerical models are used in an increasing number of applications. Most of the problems presented in this book (for example illustrated by exercises or problems) are investigated by numerical simulations. Beyond process studies (scientific understanding of the underlying processes), the models can be used for *forecast* and *impact studies*.

**Table 6.6** Model-to-data comparisons for the POLYPHEMUS system over Europe in 2001 for a few gas-phase species: number of stations (it depends on the monitoring network: EMEP and Airbase over Europe, or BDQA over France), averaged measured value ( $\mu\text{g m}^{-3}$ ), averaged simulated value ( $\mu\text{g m}^{-3}$ ), RMSE ( $\mu\text{g m}^{-3}$ ), correlation (%), MFB (%), MFE (%). Source: [126]

Species	Network	Stations	$\overline{obs}$	$\overline{y}$	RMSE	Corr	MFB	MFE
$\text{NO}_2$	EMEP	35	7.5	9.0	5.7	50.0	22	59
	AirBase	1049	23.9	15.3	14.2	57.2	-37	62
	BDQA	75	22.1	13.4	14.6	55.9	-47	70
$\text{NH}_3$	EMEP	3	7.4	6.3	5.5	28.8	12	52
	AirBase	7	12.7	6.6	13.7	27.3	-23	101
$\text{HNO}_3$	EMEP	7	0.7	1.3	1.4	26.2	40	89
$\text{SO}_2$	EMEP	43	2.0	5.3	4.9	46.7	97	106
	AirBase	992	6.5	7.3	6.6	44.2	25	70
	BDQA	10	7.8	6.8	6.5	35.7	-13	59

**Table 6.7** Statistical indicators similar to Table 6.6 for aerosols and related species

Species	Network	Stations	$\overline{obs}$	$\overline{y}$	RMSE	Corr	MFB	MFE
$\text{PM}_{10}$	EMEP	26	16.9	15.4	12.5	55.1	-9	50
	AirBase	537	25.4	15.2	17.0	44.9	-45	59
	BDQA	23	19.8	15.5	9.6	57.7	-27	41
$\text{PM}_{2.5}$	EMEP	17	12.6	8.3	8.6	54.4	-40	61
Sulfate	EMEP	57	2.5	2.0	1.7	55.6	-6	50
	AirBase	11	1.9	2.3	1.7	49.4	39	65
Nitrate	EMEP	14	2.6	4.0	3.1	41.3	30	75
	AirBase	8	3.5	4.3	2.7	71.7	6	54
Amm.	EMEP	9	1.8	2.0	1.3	51.9	19	49
	AirBase	8	1.8	2.0	0.9	74.4	14	36
Sodium	EMEP	3	1.3	2.4	2.2	62.8	47	68
Chloride	AirBase	7	0.9	3.1	3.5	69.8	83	102

- Forecast, especially for accidental releases.

The models are then supposed to be *robust*, to use small databases and to run quickly. These requirements explain that the Gaussian models are still widely used for this application. For the forecast of photochemistry, the CTMs have to be *tuned* so that a few forecast targets (such as the ozone peaks) are well reproduced. The assessment of uncertainties and the use of data assimilation methods are also frequent: a forecast system is systematically based on a strong coupling between numerical models and monitoring networks (Fig. 6.21).

Models can also provide decision-support systems, for example for the design of a monitoring network devoted to air quality or to accidental releases (this is sometimes referred to as *network design*). The numerical model is used to gener-

ate virtual situations: the optimal network is then built by minimizing a function that evaluates its performance (for detection or for data assimilation).

An illustrative example is provided by the *Comprehensive Nuclear Test Ban Treaty* (CTBT, 1996). Banning nuclear tests requires deployment of a monitoring network, so that the emission of radionuclides should be detected and the emission source localized ([158]). For another application, Fig. 6.23 shows optimized monitoring networks for the French nuclear power plants. The security and financial constraints are of course prevailing issues in such a context.

- Impact studies.

For impact studies, the numerical models are supposed to simulate long-term atmospheric compositions. Moreover, they need to describe not only the concentrations but also the sensitivity of the concentrations to emissions. This requirement motivates the use of detailed models, including all physical processes. Note that it is not obvious that the models used for forecasting are appropriate since they are often tuned to a small set of targets.

An increasing number of dispersion models are embedded in *integrated modeling* systems that provide an assessment (for instance with a monetary cost) of different scenarios of future economic activities. The typical example is the RAINS

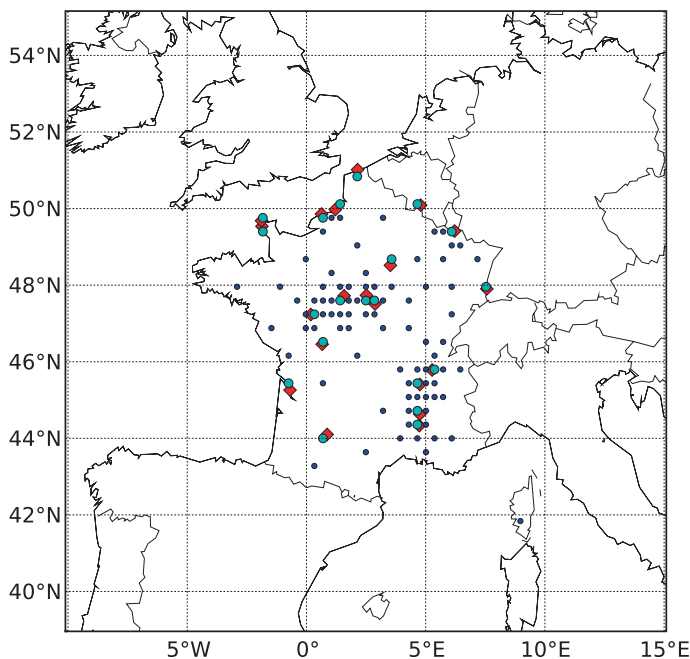


**Fig. 6.23** Optimization of a monitoring network for the French nuclear power plants. A network of 100 stations is built from the minimization of a performance function (the algorithm is simulated annealing): the 20 *rhombuses* stand for the nuclear power plants, the 20 *blue circles* stand for the “local” stations, the 80 *dark blue circles* are the other stations (chosen by the optimization procedure). The virtual accidental releases are simulated with the POLYPHEMUS system. Credit: Rachid Abida and Marc Bocquet, CEREIA

model (*Regional Air pollution INformation and Simulation*; now GAINS, *Greenhouse Gas and Air Pollution Interactions and Synergies*; [7]), used by the European Union for the CAFE process (see our Introduction). The issue is then to develop *reduced models*, accurate enough, so that they can replace the detailed physical models with a lower computational burden and for long-term studies.

## 6.5 Next-Generation Models

Air quality models are powerful tools that are increasingly used and improved. In the short term, at least five items should deeply modify the numerical models.

In the near future, a first trend will be an increase of spatial resolution. At the continental scale, the current model resolution ranges from 10 to 100 kilometers and will go down to 1–10 kilometers. This point is of course related to the improvement of meso-scale meteorological models and of emission inventories. This will induce many new open questions at the numerical level, at the parameterization level and at the data level. One may even wonder if a CTM will not use meshes similar to those used for CFD (with millions of cells and unstructured adaptative grids). This will require the use of HPCN (High Performance Computing and Networking).

The second point is related to improvement of “chemical” resolution. The complexity of physical models, especially for aerosols, will increase: a better understanding of Secondary Organic Aerosols (SOAs) implies a better representation of organic species (more variables, [46]), a coupling between organic and inorganic thermodynamics (more computational burden, [112]) and new processes (surface heterogeneous chemistry, polymerization, etc.). Apart from modeling issues, appropriate numerical algorithms will thus be required.

A third point is related to model couplings and feedbacks. This concerns for instance coupling between radiative transfer models, CTMs and meso-scale models for the radiative behavior of the atmosphere. On-line coupling will be the standard approach. Another example is provided by detailed multi-media models in the estimation of environmental impacts through multi-media models.

One must keep in mind that the final use of such models always needs a drastic reduction of CPU costs. Finding the appropriate trade-off between highly detailed physical models (the “arms race”) and tailored models that can be used in integrated modeling for impact assessment will still remain a key issue. The current situation is that one *often* uses low-level models and *sometimes* detailed models for such applications. Models of intermediate complexity or algorithms for using detailed models are therefore of great interest. The fourth point is consequently the search for reduced models to be used for integrated modeling and to be derived with a rigorous basis.

The last point is related to uncertainties. All-in-one models, tuned for a small set of target species, should be replaced by platforms able to generate a large set of models and model configurations, not only restricted to a small set of models that are based on the same assumptions. A key issue will be the ability to compute probability density functions for most outputs, in order to evaluate the *atmospheric risks*.



## Problems Related to Chap. 6

**Problem 6.1** (Variational Methods for the GDE) This problem aims at introducing the variational methods used for solving the GDE. We focus on the coagulation equation for the number distribution function,

$$\begin{aligned} \frac{\partial n}{\partial t} &= \frac{1}{2} \int_0^m K(\tilde{m}, m - \tilde{m}) n(\tilde{m}, t) n(m - \tilde{m}, t) d\tilde{m} \\ &\quad - n(m, t) \int_0^m K(m, \tilde{m}) n(\tilde{m}, t) d\tilde{m} \\ &\triangleq f(n, m, t), \end{aligned}$$

where the nucleation threshold,  $m_0$ , is supposed to be equal to 0.

Let  $V$  be a space of functions of the variable  $m$ , with an appropriate scalar product  $\langle \cdot, \cdot \rangle$ . A weak formulation of the coagulation equation is obtained by calculating the scalar product with a *test function*  $v$ :

$$\forall v \in V, \quad \left\langle \frac{dn}{dt}, v \right\rangle = \langle f(n, m, t), v \rangle.$$

$V$  is chosen so that all the integrals are well defined.

The numerical solution is defined as a *projection* of the exact solution onto a finite-dimensional subspace of  $V$ ,  $V_N$  ( $N$  stands for dimension). Let  $(L_1(m), \dots, L_N(m))$  be a basis of functions for  $V_N$ . Hence, the numerical solution can be computed as

$$\Pi n(m, t) = \sum_{j=1}^N n^j(t) L_j(m).$$

If the functions  $L_j(m)$  are piecewise polynomial functions, the method is referred to as a *finite element method*; if the functions are defined on  $[0, \infty[$ , the method is said to be a *spectral method*.

1. We investigate the so-called *spectral collocation method*. Let  $(m_i)_{i=1, \dots, N}$  be a mass discretization. The basis functions are the Lagrange polynomials:  $L_j$  is of order  $N$  and satisfies  $L_j(m_i) = \delta_{ij}$ . Formulate the system of EDOs met by  $(n^j)_j$ . Hint: choose the test functions in order to compute the *degrees of freedom*  $n^j$ .
2. Conclude for time integration. Propose a generalization for the whole GDE.

**Solution:**

1. The *test functions*  $v$  to be used for calculating the *degrees of freedom*  $n^j(t)$  are the Dirac functions  $v_i(m) = \delta(m - m_i)$ . This gives

$$\begin{aligned} \frac{dn^i}{dt} &= \sum_{j_1=1}^N \sum_{j_2=1}^N n^{j_1}(t) n^{j_2}(t) \underbrace{\left[ \frac{1}{2} \int_0^{m_i} K(\tilde{m}, m_i - \tilde{m}) L_{j_1}(\tilde{m}) L_{j_2}(m_i - \tilde{m}) d\tilde{m} \right]}_{A_{j_1 j_2}^i} \\ &\quad - n^i(t) \underbrace{\left[ \sum_{j_1=1}^N \int_0^{m_i} K(m_i, \tilde{m}) L_{j_1}(\tilde{m}, t) d\tilde{m} \right]}_{B_{i j_1}}. \end{aligned}$$

With a vectorial notation (here,  $n$  stands for the vector of components  $n^i$ ), this equation can be written as  $dn/dt = A(n)n - \text{diag}(Bn)n$  where  $[A(n)n]_i = n^T A^i n$ . The matrices  $(A^i)_i$  and  $B$  can be computed in a preprocessed step.

2. The time integration of the resulting system of EDOs can be carried out with an appropriate scheme. The method is easily generalized to the whole GDE. This can avoid the use of a splitting method for the three processes (coagulation, condensation and evaporation, nucleation). Due to the wide range of timescales for condensation, the time integration scheme must be implicit.

This framework is more powerful than the sectional methods since it provides a functional description of  $n(m, t)$ : on the contrary, a sectional method computes only values at the discretization points  $(m_i)_i$  (and not at any  $m$ ).

To know more ([32]):

E. DEBRY AND B. SPORTISSE, *Numerical simulation of the General Dynamics Equation (GDE) for aerosols with two collocation methods*, Appl. Numer. Math., **457** (2007), pp. 885–898

**Problem 6.2** (Adjoint Model for the Dispersion Equation) This problem illustrates the notion of an *adjoint model* for the linear case. We consider the dispersion of a passive tracer (let us say a radionuclide). The time evolution of the mixing ratio is governed by

$$\frac{\partial C}{\partial t} + V \nabla C = \frac{1}{\rho} \text{div}(\rho K \nabla C) - \lambda C + S,$$

where  $S$  is a point source term. The coefficient  $\lambda$  describes all the linear loss terms (scavenging and filiation). We suppose that  $C(t = 0) = 0$  and  $\nabla C = 0$  along the boundaries of the spatial domain  $\Omega$ . The time interval is  $[0, T]$ .

The solution  $C$  depends on the source term  $S$  and is written as  $C_S$ . This defines the so-called *forward model*: a given source term generates a mixing ratio field. Let  $J$  be a function of the source term defined by

$$J(S) = \iint e(x, t) \rho(x, t) C_S(x, t) dx dt,$$

with  $e(x, t)$  a sampling function (with respect to time and space). The integration is carried out over  $\Omega \times [0, T]$ . In practice,  $J$  represents the observation of the mixing ratio at a given point or the averaged value.

1. Prove that  $J$  is a linear function of  $S$ .
2. It is desired to calculate the sensitivity of  $J$  with respect to the source term (e.g. for inverse modeling). Formulate the equation satisfied by  $\nabla_S J$ , defined for any perturbation of the source term  $\delta S$ , by

$$J(S + \delta S) = J(S) + \iint \rho(x, t) \nabla_S J \delta S(x, t) dx dt$$

Is the resulting algorithm efficient?

3. We start with a simple formal calculation in order to introduce a more powerful approach. Let  $\langle \cdot, \cdot \rangle$  be the scalar product defined by the air density  $\rho$ :  $\langle f, g \rangle = \iint \rho f g \, dx dt$ . The dispersion model generates a linear operator  $M$  to be applied to the source term  $S$ , so that  $C_S = MS$ . Thus,

$$J(S) = \langle MS, e \rangle = \langle S, M^T e \rangle,$$

where the definition of the transpose matrix (the *adjoint* matrix) is used. Upon identification,  $\nabla_S J = M^T e$  since  $J(S) = \langle S, \nabla_S J \rangle$ , which provides a direct computation of the gradient.

The difficult point is to give a meaning for the *adjoint model*  $e \rightarrow M^T e$ . Let  $C^*$  be a spatial field (to be made precise below). Upon integration of the dispersion equation multiplied by  $\rho C^*$ , formulate an evolution equation for  $C^*$  (the so-called *adjoint variable*) so that

$$J(S) = \langle C^*, S \rangle = \iint \rho C^* S \, dx dt.$$

Hints: use integration by parts and anneal all the terms related to boundary conditions (justified by conditions to be applied to  $C^*$ ).

4. Comment. Is it possible to reuse the initial model to compute  $C^*$ ?

**Solution:**

1.  $C_S$  is a linear function of  $S$ . This implies the linearity of  $J$ .
2. We easily obtain

$$\begin{aligned} \iint \rho(x, t) \nabla_S J \delta S(x, t) \, dx dt &= J(S + \delta S) - J(S) \\ &= \iint \rho(x, t) e(x, t) C_{\delta S}(x, t) \, dx dt, \end{aligned}$$

with  $C_{\delta S} = C_{S+\delta S} - C_S$  governed by the linear dispersion equation.

This approach is not efficient because this does not provide  $\nabla_S J$ . It is only possible, for any perturbation  $\delta S$ , to get  $\iint \rho \nabla_S J \delta S \, dx dt$ , which requires that we solve the model for any perturbation. Upon spatial discretization, with  $n$  grid cells at ground (this means  $n$  point source emissions), this requires  $n$  model runs for computing  $\nabla_S J$  (one model run per gradient component)! This is not affordable in practice.

3. Upon integration by parts, the equation yields

$$\begin{aligned} \langle C^*, S \rangle &= \iint \rho C^* \left( \frac{\partial C}{\partial t} + V \nabla C - \frac{1}{\rho} \operatorname{div}(\rho K \nabla C) + \lambda C \right) \, dx dt \\ &= \iint \left( -\frac{\partial(\rho C^*)}{\partial t} C - \operatorname{div}(\rho V C^*) C - C \operatorname{div}(\rho K \nabla C^*) + \rho \lambda C^* C \right) \, dx dt, \end{aligned}$$

thus

$$\langle C^*, S \rangle = \iint \underbrace{-\left( \frac{\partial \rho}{\partial t} + \operatorname{div}(\rho V) \right)}_{=0} C^* C \, dx dt$$

$$\begin{aligned}
& + \iint \rho C \left( -\frac{\partial C^*}{\partial t} - V \nabla C^* - \frac{1}{\rho} \operatorname{div}(\rho K \nabla C^*) + \lambda C^* \right) dx dt \\
& = \left\langle C, -\frac{\partial C^*}{\partial t} - V \nabla C^* - \frac{1}{\rho} \operatorname{div}(\rho K \nabla C^*) + \lambda C^* \right\rangle.
\end{aligned}$$

The terms related to initial and boundary conditions can be omitted if  $C^*(t = T) = 0$  and  $\nabla C^* = 0$  along the domain boundaries. As  $J(S) = \langle C, e \rangle$ , we get  $J(S) = \langle C^*, S \rangle$  if  $C^*$  is governed by

$$-\frac{\partial C^*}{\partial t} - V \nabla C^* = \frac{1}{\rho} \operatorname{div}(\rho K \nabla C^*) - \lambda C^* + e(x, t).$$

This is a PDE with a backward time integration (which justifies the condition at  $t = T$ ). This equation gives a meaning to  $M^T e$ , defined as  $C^*$ .

4. The dispersion equation for  $C^*$  can be solved by using the initial model: the time sequence has to be reversed for the forcing fields, the sign of the wind velocity has to be reversed and the source term is  $e(x, t)$ . Thus, the solution is  $C^*$ .

The sensitivity analysis is easy to carry out because only *one* model run is required for computing  $\nabla_S J = C^*$ . This result does not depend on the dimension of  $S$ !

This approach can be extended to the nonlinear case. The adjoint model is a powerful approach to be used for computation of the gradient of a scalar value with respect to input data fields (gridded values). Note that this can be used for computing the gradient of the cost function in variational data assimilation methods. Building the *adjoint code* from a nonlinear code is not easy. *Automatic differentiation techniques* are a promising tool.

*To know more* ([95, 55]):

G. MARCHUK, *Mathematical models in environmental problems*, vol. 16, North-Holland, 1986

F. HOURDIN AND J.-P. ISSARTEL, *Sub-surface nuclear tests monitoring through the CTBT <sup>133</sup>Xe network*, Geophys. Res. Lett., **27** (2000), pp. 2245–2248



<http://www.springer.com/978-90-481-2969-0>

Fundamentals in Air Pollution

From Processes to Modelling

Sportisse, B.

2010, X, 299 p., Hardcover

ISBN: 978-90-481-2969-0